Ion mobility in crystalline battery materials

Mohsen Sotoudeh,[†] Sebastian Baumgart,[†] Manuel Dillenz,[†] Johannes Döhn,[†] Katrin Forster-Tonigold,[‡,¶] Katharina Helmbrecht,[†] Daniel Stottmeister,[†] and Axel Groß[*,†,‡]

[†]*Institute of Theoretical Chemistry, Ulm University, 89081 Ulm, Germany*

[‡]*Helmholtz Institute Ulm (HIU), Electrochemical Energy Storage, 89081 Ulm, Germany*

[¶]*Karlsruhe Institute of Technology (KIT), P.O. Box 3640, D-76021 Karlsruhe, Germany*

E-mail: axel.gross@uni-ulm.de

Abstract

Ion mobility in electrolytes and electrodes is an important performance parameter in electrochemical devices, particularly in batteries. In this review, we concentrate on the charge carrier mobility in crystalline battery materials where the diffusion basically corresponds to hopping processes between lattice sites. However, in spite of the seeming simplicity of the migration process in crystalline materials, the factors governing mobility in these materials are still debated. There are well-accepted factors contributing to the ion mobility such as the size and the charge of the ions, but they are not sufficient to yield a complete picture of ion mobility. In this review, we will critically discuss possible factors influencing ion mobility in crystalline battery materials. To gain insights in these factors, we discuss chemical trends in batteries, both as far as the charge carriers as well as the host materials are concerned. Furthermore, we will also address fundamental questions, for example about the nature of the migrating charge carriers.

1 Introduction

Ion mobility is a critical performance parameter not only in electrochemical energy storage and conversion but also in other electrochemical devices. It is of particular importance in solid electrolytes and electrode materials. A thorough understanding of the basic principles underlying the ion mobility in crystalline materials is not only interesting from a fundamental, but also from a applied point of view ,[1] as for example the reduced performance of batteries at low temperatures is supposed to be related to low ion mobility. In recent years, significant progress has been made in our conceptual understanding of ion mobility in crystalline electrode materials, especially concerning the role of non-ionic interaction between the migrating ion and the host lattice .[2–5] In this review, we will discuss the materials properties that correlate with ionic conductivity, in particular with the height of the activation barrier, using the descriptor concept. Both experimental and theoretical studies will be addressed in order to establish strategies to identify solid electrolytes and electrodes with improved mobility mobility.

This review is concerned with the ion mobility in crystalline battery materials, including both, electrolytes and electrodes. There is a fundamental difference between electrolytes and electrodes: electrolytes are ion conductors, but they should be electronic insulators, otherwise no electrons would flow through an outer circuit upon battery operation. Electrodes, on the other hand, should be both ion- as well as electron-conductors, otherwise the recombination of ions and electrons upon entering electrodes would not be possible. Still, from a quantum chemical perspective, there is no fundamental difference in the determination of migration properties which crucially depend on the minimum energy path connecting two equivalent intercalation sites and the maximum activation barrier along this path.

The nature of the migrating species and the overall charge state are related topics that need to be discussed. Is the migrating species in solid electrolytes really an ion or rather an atom? We will address this issue by discussing various charge partition schemes which are supposed to determine the charge state of atoms in a chemical environment. A basic

notion of macroscopic materials is that they are typically charge-neutral. This concept is well-known from liquid electrolytes where the charge of any solvated ion is compensated by a corresponding counter ion. Solid electrolytes are often coined "single-ion conductor". If these materials are single ion conductors, the natural question arises: What is counter ion in these single ion materials? Furthermore, ion mobility might not just proceed via the hopping of single ions, there might be also concerted processes involved in these processes.

There is a wide class of different crystalline materials used in batteries such as spinels, perovskites, olivines, Prussion blue, NASICON, Chevrel phase, layered oxides, and van der Waals bonded layered systems. Apart from the structural differences of all these material classes, the interaction of the migrating ion with these different host lattices differs to a certain extent as well. Hence we will dedicate a full section to each of these materials classes.

A very helpful tool to understand the principles underlying material properties is the descriptor concept, which can be regarded as the relation between desired or undesired features such as the ion mobility with basic material properties. Once such a descriptor has been successfully established, the search for materials with desired functional properties can be significantly facilitated as there is no longer the need to perform numerous time-consuming experiments or numerically challenging quantum chemical calculations. However, identifying descriptors can not been fully separated from the fundamental issues discussed above as the very existence of a descriptor already reflects the presence of a fundamental principle underlying the existence of this descriptor.

2 Obstacles for ion mobility within crystals

In this review, we concentrate on the ion mobility in single crystals. Still, macroscopic solid materials are typically no single crystals but have a fine structure. There are further structural factors that might influence the ion mobility.

- Electrochemical reactions at interfaces: In battery systems, crystalline materials interface with other components such as electrolytes, as shown in Figure 1. Unfavorable interfacial reactions, such as the formation of a passivation layer or a high interfacial resistance, can impede ionic transport across the interfaces, resulting in a reduced battery performance.

- Grain boundaries: Polycrystalline materials, as employed in batteries, contain grain boundaries, which can act as barriers for ion migration, as schematically shown in Figure 1. These boundaries can also impede ion mobility and increase resistance to ion transport, limiting the overall performance and stability of the battery. Controlling and minimizing these boundaries is crucial for improving ion mobility. Note that the formation energies of point defects in the grain boundary are lower compared to the bulk lattice. Vacancies and interstitials have similar formation energies, indicating their equal importance in grain-boundary diffusion. Additionally, the diffusion anisotropy is influenced by the grain-boundary structure, with faster or slower diffusion occurring along the tilt axis in tilt boundaries compared to diffusion normal to the tilt axis.

- Defects and Impurities: Crystal defects, such as vacancies or interstitials, can disrupt the regular lattice structure and hinder or facilitate ion mobility. Additionally, impurities or dopants present in the crystal can alter the electronic properties and affect the mobility of ions.

- Anisotropic diffusion: Crystalline materials often exhibit anisotropic diffusion, meaning that ion mobility may vary significantly along different crystallographic directions. This anisotropy can result in an uneven distribution of charge carriers and lead to localized regions of high current density, which can promote side reactions, electrolyte decomposition, and even structural degradation of the material.

- Structural constraints: Crystal lattice constraints restrict the movement of ions within the material. The fixed crystal lattice can hinder the diffusion of ions, leading to lower

ion mobility. This can result in slower charge/discharge rates and reduced overall battery performance.

Addressing these challenges requires a combination of materials design, synthesis techniques, and understanding of the fundamental mechanisms governing ion transport in crystalline materials. Strategies such as doping, nanostructuring, and interface engineering can be employed to enhance the ion mobility and improve the performance of crystalline materials in batteries. Still, it should be noted that typically the properties within the crystalline parts of a macroscopic material represent a lower bound for the ion mobility. Hence a material which already has a low ion mobility as a single crystal should be disregarded as a promising material with respect to its migration properties.

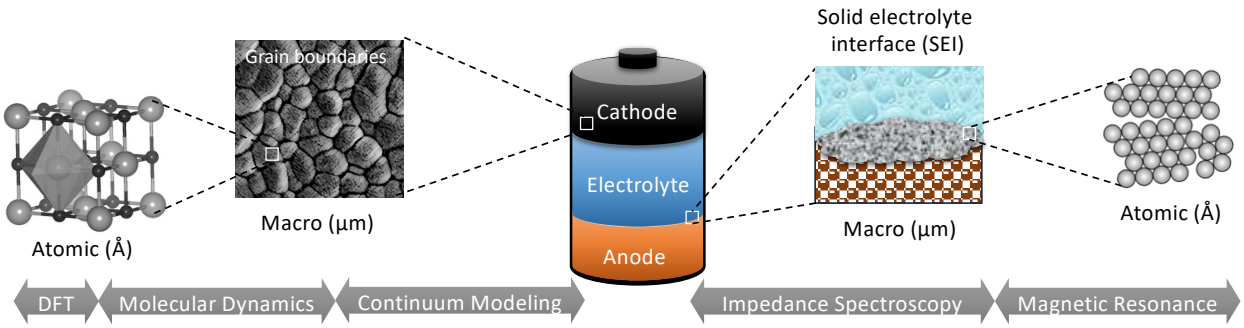

Figure 1: Schematic illustration of the relevant scales and configurations explored within a battery material. The method utilized to calculate ion transport properties in the respective length scales are indicated by grey arrows, namely Density Functional Theory (DFT) and Molecular Dynamics (MD) simulations. The experimental techniques employed to directly probe ion transport are also aligned with their corresponding length scales.[6] The figure illustrates the diverse range of scales, from atomic to mesoscale, and the corresponding configurations occurring in a battery. Investigating battery materials in such a way will lead to improve performance characteristics for future battery generation.

3 Fundamental mechanisms of ion mobility

In a crystal, the collective displacement of an atom is caused by numerous individual jumps of specific length. Fundamentally, an atom undergoes movement towards an adjacent location, which can either be a neighboring vacancy or an interstitial site. It is evident that the

moving atom must navigate through the intervening lattice atoms, requiring energy to overcome activation barriers along the migration path which necessitates energy for this process. Typically, the energy needed to activate the jump is considerably greater than the thermal energy k_BT.

At finite temperatures, atoms within a crystal oscillate around their equilibrium positions. Usually, these oscillations lack the necessary intensity to overcome the barrier, causing the atom to revert back to its original position. Occasionally, substantial displacements occur, resulting in a successful diffusion of the atom. These occurrences of activation are infrequent compared to the frequencies of the lattice vibrations, which are characterized by the Debye frequency, typically ranging from 10^{12} to 10^{13} s^{-1}. Once an atom has moved due to an activation event, the energy dissipates quickly. Consequently, the atom becomes deactivated and awaits many lattice vibrations on average before it jumps again. In a crystal, atoms undergo thermally activated motion, transitioning between lattice sites (or interstitial sites) through a sequence of distinct jumps.

The concept of atomic movement between neighboring sites was initially proposed by Wert,[7] and has since been further developed by Vineyard.[8] Vineyard's method builds upon the canonical ensemble of statistical mechanics, which considers the distribution of atomic positions and velocities. The process of an atomic jump can be understood as taking place within an energy landscape defined by the disparity in Gibbs free energy (G^{migr}) between the saddle-point barrier and the equilibrium position. Here, G^{migr} represents the Gibbs free energy of atom migration (denoted as superscript $migr$) and can be divided into

$$G^{migr} = H^{migr} - TS^{migr} \tag{1}$$

where H^{migr} represents the enthalpy associated with the migration, while S^{migr} represents the entropy related to the migration. Through the application of statistical thermodynamics,

Vineyard[8] demonstrated that the jump rate (ω), which signifies the number of jumps per unit time to an adjacent site, can be expressed as

$$\omega = \nu^0 \exp(-\frac{G^{migr}}{k_B T}) = \nu^0 \exp(\frac{S^{migr}}{k_B T}) \exp(-\frac{H^{migr}}{k_B T}). \tag{2}$$

The attempt frequency, denoted as ν^0, is commonly referred to as the Debye frequency, which signifies the oscillation frequency occurring near the equilibrium position along the reaction pathway. k_B is the Boltzmann constant, and T denotes the absolute temperature. The entropy of migration signifies the alteration in lattice vibrations that accompany the displacement of the jumping atom from its equilibrium state to the saddle point configuration. In the Vineyard approach, the probability of reaching the transition state is derived by comparing the configurational partition functions of the initial state and the transition state, while the rate of crossing is determined by the one-way forward flux at the transition state. The expression for the migration entropy, in harmonic approximation, is therefore given by:

$$S^{migr} = k_B \left[\sum_{j=1}^{3N} \ln \left(\frac{h\nu_j}{k_B T} \right) - \sum_{j=1}^{3N-1} \ln \left(\frac{h\nu'_j}{k_B T} \right) \right]. \tag{3}$$

The frequencies ν_j represent the $3N$ normal modes for vibrations around the equilibrium site, while the $3N-1$ frequencies ν'_j correspond to the vibrations at the saddle point perpendicular to the jump direction with the constrained motion.

The macroscopic diffusivity is then obtained from the barrier of the single diffusion event by transition state theory (rate theory).[9] Assuming $h\nu \gg k_B T$, the effective frequency $\nu^* = \nu^0 \exp(S^{migr}/k_B T)$ in the Arrhenius expression is obtained from the ratio of the product of the $3N$ normal frequencies of the entire crystal at the initial configuration of a transition to the product of the $3N-1$ normal frequencies of the crystal when it is constrained in a

saddle point configuration:[8]

$$\omega = \frac{1}{2\pi} \frac{\prod_{j=1}^{3N} \nu_j}{\prod_{j=1}^{3N-1} \nu'_j} \exp\left(-\frac{H^{migr}}{k_B T}\right) = \nu^* \exp\left(-\frac{H^{migr}}{k_B T}\right). \tag{4}$$

On the macroscopic scale, the diffusion coefficient (D) is described by Fick's first law of diffusion:

$$\vec{J} = -D\vec{\nabla}c. \tag{5}$$

where $\vec{J}$ is the diffusion flux, which is the amount of substance (e.g., ions) passing through a unit area per unit time, and D is the diffusion coefficient, representing the proportionality constant between the diffusion flux and the concentration gradient ($\vec{\nabla}c$). The units of the diffusion coefficient are typically square units of length per unit time (e.g., cm^2/s or m^2/s). The diffusion coefficient is a measure of how quickly particles (atoms, or ions) move through a medium due to random thermal motion. It quantifies the rate at which particles spread out from areas of high concentration to areas of low concentration. It is important to realize that this chemical diffusion differs from the tracer or Einstein diffusion, which is due to thermal fluctuation. Only a low concentrations of the diffusing particles, the chemical and the tracer diffusion coefficients are the same.

Ionic conductivity, on the other hand, is a measure of how well a material conducts electric current through the movement of charged ions. It is an important property in the context of electrolytes, which are substances that can conduct electricity when dissolved in a solvent or when in a molten state. Ionic conductivity (σ) is described as product of the concentration of mobile ions c, the charge of the ions q and the mobility μ of the charge

carrier:

$$\sigma = qc\mu. \tag{6}$$

The unit of the ionic conductivity is typically Siemens per meter (S/m). Note that the diffusion coefficient at low particle densities relates to the movement of particles in a medium due to random motion, while ionic conductivity refers specifically to the ability of a material to conduct electric current through the movement of charged ions. Both properties are important in understanding ionic transport and are relevant in different scientific and technological applications.

The thermal dependency of the ionic conductivity is given by:

$$\sigma = \frac{\sigma_0}{k_B T} \exp\left(-\frac{H^{migr}}{k_B T}\right) \approx \frac{\sigma_0}{k_B T} \exp\left(-\frac{E_a}{k_B T}\right) \tag{7}$$

where the pre-exponential factor σ_0 accounts for the entropy of migration, the jump distance, the attempt frequency and a factor depending on the reaction mechanism. The height of the activation barrier is given by E_a. Besides, if non-interacting charge carriers are considered, the ionic conductivity can be expressed in terms of the diffusion coefficient D, by employing the well-known Nernst-Einstein relationship

$$D = \frac{\sigma}{cq^2} H_r \, k_B T \tag{8}$$

where H_r is the Haven ratio, which depends on the specific diffusion mechanism.

Defects within crystalline solids can exhibit a strong impact on the ionic conductivity of the material. In 1926, the pioneering work of the Russian scientist Frenkel[10] marked the introduction of the point defects concept. Frenkel proposed that the movement caused by thermal agitation leads to atom transitions from their regular lattice positions to interstitial sites, resulting in the creation of lattice vacancies. This phenomenon is now known as Frenkel

defect, which already encompassed the notions of vacancies and self-interstitials. In the early 1930s, Wagner and Schottky[11] expanded on this idea by investigating the general occurrence of disorder in binary AB compounds, considering the presence of vacancies, self-interstitials, and defects where atoms occupy the wrong sublattices.

The periodicity of the lattice in a defect-free crystal determines the mass and charge density. However, the introduction of a point defect disrupts this regular pattern. In metals, the presence of conduction electrons enables effective electronic screening of defects, resulting in uncharged point defects. Conversely, in ionic crystals, the formation of a point defect, such as a vacancy in one sublattice, disturbs the overall charge neutrality. To maintain charge balance, defect populations in ionic crystals can exhibit Frenkel disorder or Schottky disorder. Frenkel disorder involves an equal number of vacancies and self-interstitials in one sublattice, while Schottky disorder entails an equal number of vacancies in both, the cation- and anion-sublattices. For instance, in compounds like NaCl, which consists of cations and anions with opposite charges of equal magnitude, the number of vacancies in each sublattice must be equal to ensure charge neutrality. In semiconductors, point defects introduce energy levels within the band gap, and their charge state (neutral or ionized) depends on the position of the Fermi level. In the subsequent sections, we will first examine point defects in metals, and ionic crystals before going on to semiconductors.

3.0.1 Metals

Point defects play a crucial role in the diffusion processes within crystalline solids. This significance stems from two primary characteristics. Firstly, point defects possess the ability to traverse the crystal lattice and facilitate the diffusion of atoms, essentially acting as carriers for this process. Secondly, these defects exist in a state of thermal equilibrium. In a crystal without defects, the mass and charge density exhibit periodicity in accordance with the lattice structure. The introduction of a point defect disrupts this periodicity. In metals, the conduction electrons effectively screen defects, resulting in uncharged point defects within

the metal.

Diffusion in metals occurs when individual atoms or ions move from one location to another within the metal's crystal lattice, involving the movement of atoms from lattice sites to nearby vacant sites as well as migrating into interstitial sites between existing lattice atoms.[12] This process happens due to thermal energy, which causes the atoms or ions to vibrate. When atoms gain sufficient energy, they can overcome the forces holding them in place and move to neighboring lattice sites. The diffusion of atoms in metals is influenced by various factors, including temperature, concentration gradients, and the presence of defects in the crystal lattice.[13] At higher temperatures, atoms have more thermal energy, leading to increased diffusion rates. Concentration gradients also drive diffusion, as atoms tend to move from regions of higher concentration to regions of lower concentration to achieve a more uniform distribution. Diffusion in metals plays a crucial role in determining material properties, such as hardness, electrical conductivity, and corrosion resistance. For metal anodes in batteries, it should be mentioned that there is no mobility needed as the metal anode is either formed or dissolved upon charging or discharging, respectively.

3.0.2 Ionic Compounds

Ionic compounds, such as alkali halides, exhibit a fixed stoichiometry and possess a broad band-gap, rendering thermally generated electrons or holes negligible. These materials represent the traditional group of ion conductors, where conductivity originates from the existence and movement of vacancies and/or self-interstitials. A well-known example is silver iodide, for which fast ionic conduction was reported in 1914.[14]

In an ionic crystal, there is a limitation on the type and quantity of defects that can arise, as they require an equal count of cation and anion atoms in their structure. Subsequently, only defect populations that maintain charge neutrality can emerge. Furthermore, there is no need to take into account the formation of antisite defects, given the substantial Coulomb energy required for an ion to be situated in the incorrect sublattice.

Suppose the formation of vacancies and self-interstitials in the sublattice, arising from cations occupying cation sites. This particular disorder is referred to as Frenkel disorder. Frenkel pairs are used to denote the combination of vacancies and self-interstitials. For undoped crystals to maintain charge neutrality, it is necessary for the quantities of vacancies and self-interstitials to be balanced and equal. The occurrence of Frenkel disorder can be observed within the silver sublattices of both silver chloride and silver bromide.[15,16]

Schottky disorder occurs when an equal number of vacancies are formed in both sublattices. In an undoped crystal, maintaining charge neutrality necessitates having equivalent concentrations of cation and anion vacancies. In the majority of alkali halides and numerous oxides, it has been observed that Schottky disorder is the primary factor influencing the distribution of defects.

3.0.3 Semiconductors

Semiconductor crystals provide a larger volume for the presence of self-interstitials compared to densely packed ionic structures. The formation enthalpies of vacancies and self-interstitials in semiconductors exhibit similar values. In the case of silicon, both self-interstitials and vacancies coexist in a state of thermal equilibrium and play significant roles in self-diffusion and solute diffusion processes. Conversely, in germanium, vacancies take precedence in thermal equilibrium and seem to be the sole defect relevant to the diffusion. Semiconductors can possess either neutral point defects or defects in different electronic charge states, as these defects create energy levels within the band-gap of the semiconductor. The neutrality or ionization of a defect is determined by the position of the Fermi level. A considerable dopant concentration significantly influences the diffusion process in semiconductors by utilizing defects with different charge states as carriers for diffusion. At lower temperatures, the impact of doping on diffusion becomes more noticeable as the intrinsic carrier density becomes exponentially suppressed upon lowering the temperature.

3.1 Crystalline electrodes vs. crystalline electrolytes in battery materials

Up until now, the focus of the discussion has been centered on mobility in solid substances. In electrodes the insertion of the "ions" = atoms occurs under conditions in which this insertion is thermodynamically favorable, playing a crucial role in determining the voltages and capacities of electrochemical cells. Often, when talking about electrolytes, it is assumed that they are liquids. However, it's worth noting that there are also various solid materials capable of fulfilling the main functions of an electrolyte. These solids enable the movement of charged ionic species while selectively impeding the transport of electronic species. Although there are numerous materials that effectively insulate against electronic currents, what sets apart materials capable of acting as a solid electrolyte is the high mobility of ionic species within their crystal structures.

AgI was one of the first solid-state ion conductors to exhibit high ionic conductivity. It was followed by the development of sodium-ion-conducting β-alumina and NASICON, and later, several fast lithium-ion conductors were discovered. Recent studies suggest that divalent cations, such as Mg^{2+} in mixed electron- and ion-conducting $Mg_xMo_6X_8$ (X = S or Se) (see Chapter 5.6) and ion-conducting metal borohydrides like $LiBH_4{\cdot}CH_3NH_2$[17] or $Mg(BH_4)_2{\cdot}(NH_3)$,[18] can demonstrate reasonable mobility in solids. In the latter structures, the metal is coordinated by four borohydride complexes containing BH_4^- bridges between two metal atoms. Additional neutral molecules like NH_3 or CH_3-NH_3 can be introduced to interrupt the metal and BH_4^- network by forming N-$H^{\delta+}$ ... $^{-\delta}$H-B dihydrogen bonds to interlink the remaining -BH_4-Mg-BH_4- chains. Additionally, various anionic species can exhibit mobility in halides and oxides, such as oxygen-ion conductors at elevated temperatures. The polyhedral network comprises numerous metal and nonmetal ions, with chalcogens, halogens, and nitrogen serving as ligands. Polyhedra composed of early transition-metal ions from the first and second rows, such as Ti^{4+}, Zr^{4+}, Nb^{5+}, or Ta^{5+}, along with ions from groups 13, 14, and 15, are employed to form different coordination arrangements with the ligand. These

polyhedra can form the backbone of the crystals in various configurations, such as isolated polyhedral units as seen in γ-Li_3PO_4, corner sharing as in NASICON, or edge/corner sharing as in garnets. The subsequent sections will provide further details on these ionic conductors.

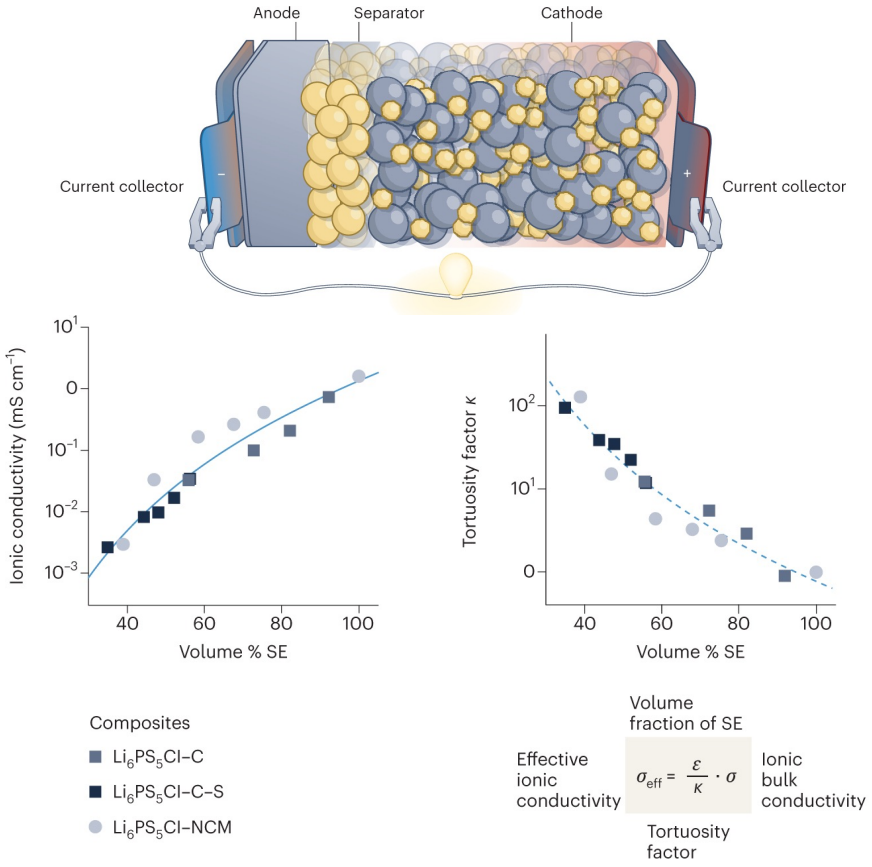

Figure 2: Schematic illustration of the generalized lithium solid-state battery (SSB) cell concept. Bottom graphs show the analysis of the partial lithium-ion conductivity (σ_{eff}) and the assessment of the tortuosity factor (κ) based on the weight fraction of the SE (Solid Electrolyte), which correlates with the volume fraction (ε). The graphs are taken from.[19]

Developing solid-state batteries (SSBs) requires thick cathode architectures and low solid electrolyte (SE) fractions in order to achieve high energy density, as illustrated in Figure 2. It has recently been demonstrated that reducing the volume fraction of the solid electrolyte in the composite significantly decreases the effective ionic conductivity of inorganic SEs compared to their bulk conductivity,[19] as shown in Figure 2. In addition, solid electrolytes need effective conductivities above 10 mS cm^{-1} to achieve fast rates in cathode composites. If completely solid cathodes cannot meet performance or long-term operation requirements, hybrid

electrolytes or liquid electrolytes (LEs) may be employed, so-called almost solid electrolytes. Lowering lithium content and finding less critical compositions in SEs, along with optimized composite route preparation, is crucial for SSBs to effectively replace lithium-ion batteries (LIBs). Although considered safer, the increased safety of SSBs needs unequivocal proof, as there are potential safety risks associated with short circuits, toxic SEs, and percolation of the liquid electrolytes to the anode. Note that binaries are simple compounds that can be used as coating materials to prohibit elecrolyte degradation. In particular halides have been identified as suitable coating materials due to their favorable electrochemical stability together with exhibiting a suitable ionic mobility.[20–22]

Ternary materials such as inorganic oxides,[23,24] hydrides,[25–27] and chalcogenides[2,22,28–30] display commendable bulk ionic conductivities. Among these, chalcogenide spinel lattices have been recognized as ionic conductors with high ion mobility,[28,30] a crucial property for solid electrolytes. Spinel compounds, including transition metals like Cr and Mn, possess high binding energies[31] and satisfactory electron conductivity, rendering them appropriate cathode materials. Conversely, closed-shell systems like Sc and Y exhibit relatively low electron conductivity, qualifying them for use as solid electrolytes.[2,22,28]

Despite the wide electrochemical stability window observed in many solid-state electrolytes, several fast ion conductors discovered so far remain unstable at low potentials when paired with negative electrodes like graphite and metallic lithium. This necessitates the use of alternative electrode materials like titanates. In addition, fast ion conductors can also react with positive electrode materials, leading to sluggish interfacial charge-transfer kinetics. While the substitution of elements within a specific structural family can enhance ionic conductivity, there is a lack of comprehensive knowledge to establish a universal guide for fast ion conductors across various structural families. Consequently, predicting the most conductive structure/composition is challenging, impeding the design of new or multilayer ionic conductors that exhibit improved conductivity and stability, meeting the requirements of solid-state batteries. Therefore, further research is necessary to investigate trends and

mechanisms in ionic conductivity among different classes of ion conductors. This will offer valuable insights into universal descriptors of ionic conductivity and facilitate the design of advanced ionic conductors.

3.2 Diffusion mechanisms

The initial step in understanding atom diffusion within solids involves examining the various mechanisms of diffusion that come into play.

3.2.1 Interstitial Mechanism

In materials allowing interstitial diffusion, migrating atoms can be incorporated into the interstitial sites of the host lattice to form a solid solution known as an interstitial solid solution. The interstitial sites are determined by the host lattice's geometry. In lattices such as fcc and bcc, the interstitial solutes typically occupy octahedral and/or tetrahedral interstitial sites. The diffusion of an interstitial solute occurs when it jumps from one interstitial site to an adjacent site. This mechanism is referred to as interstitial diffusion, as illustrated in Figure 3.

The migration path of an interstitial atom begins at an equilibrium position, from where the atom moves to the configuration known as the transition state (saddle point) where the lattice experiences maximum strain, as this is the energetically least favorable position along the migration path and then moves to a neighboring interstitial position. In the saddle-point configuration, the surrounding matrix atoms need to move aside to allow the passage for the migrating atom. Conceptually, this represents the most straightforward diffusion mechanism. It is alternatively referred to as the direct interstitial mechanism. Diffusion coefficients for atoms undergoing migration through the direct interstitial mechanism typically exhibit relatively high values because the interstitial atom does not have to wait for a defect to align in order to execute a jump. This mechanism is relevant for the migration of small atoms that can easily occupy interstitial positions and which do not significantly disturb the atoms

of the host material from their normal lattice positions when they move.

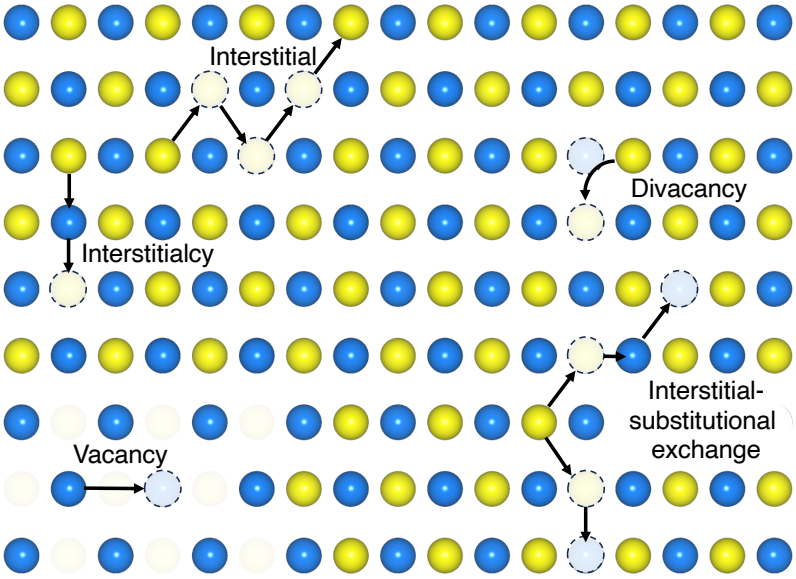

Figure 3: Schematic depiction of the different mechanisms of ion migration. The arrows illustrate five separate, common migration mechanisms: the vacancy mechanism (lower left), the direct interstitial mechanism (top left), interstitialcy mechanism (middle left), the divacancy mechanism (top right) representative for all multivacancy mechanisms and the interstitial-substitutional exchange mechanism (bottom right). The circles represent framework atoms and charge carrier atoms in blue and yellow, respectively. Vacant sites are indicated by a dotted circle, while atoms that are faded out without any feature are marked as not existent.

3.2.2 Vacancy Mechanism

In the vacancy mechanism, the propagation of an atom proceeds through migration along vacancy sites, as shown in Figure 3. This mechanism has been acknowledged as the primary means for the diffusion of matrix atoms and substitutional solutes in metals. Furthermore, its applicability extends to the diffusion phenomenon observed in various ionic crystals, ceramic substances, and even germanium.

3.2.3 Divacancy Mechanism

Diffusion can take place through clusters of vacancies, such as divacancies, trivacancies etc., as long as the formation of these agglomerates is energetically feasible, as illustrated in Fig-

ure 3. In thermal equilibrium, there is always a non-zero statistical probability that monovacancies meet and form divacancies. As temperature increases, the concentrations of both mono- and divacancies at equilibrium also rise. However, the concentration of divacancies increases statistically more rapidly, thus becoming significant at high temperatures. In addition, divacancies in fcc metals exhibit greater mobility than monovacancies. Consequently, self-diffusion in fcc metals generally involves contributions from both the monovacancy and divacancy mechanism. Apart from these differences, the two mechanisms strongly resemble each other. The influence of bound trivacancies on diffusion is usually considered negligible.

3.2.4 Interstitialcy Mechanism

Diffusion can take place through the interstitialcy mechanism, also known as the indirect interstitial mechanism, when an interstitial atom has approximately the same size as the lattice atoms or the lattice atoms within a specific sublattice of a compound. In this mechanism, a (self) interstitial atom replaces an atom located at a substitutional site, which in turn displaces a neighboring lattice atom, as illustrated in Figure 3. It is worth noting that non-collinear variations of the interstitialcy mechanism, where atoms move at an angle to each other, can also occur. These mechanisms are considered collective mechanisms because they involve the simultaneous movement of at least two atoms.

In metals, the contribution of the interstitialcy mechanism to thermal diffusion is insignificant. This is due to the relatively high formation enthalpies of self-interstitials when compared to vacancies. However, the interstitialcy mechanism plays a crucial role in radiation-induced diffusion. When a crystal is subjected to energetic particles such as protons, neutrons, or electrons, the atoms within the lattice are displaced from their original positions, resulting in vacancies. Simultaneously, the displaced atom becomes a self-interstitial as it is embedded back into the lattice. Consequently, pairs of vacancies and self-interstitials, known as Frenkel pairs, are created without thermal activation. Once these defects gain mobility, they facilitate diffusion and contribute to radiation-induced diffusion, which pertains to the

study of crystal damage caused by radiation.

3.2.5 Interstitial-substitutional Exchange Mechanisms

Solute atoms have the ability to dissolve in a solvent crystal on interstitial sites as well as substitutional sites. These solutes, known as 'hybrid solutes', can then undergo diffusion through interstitial-substitutional exchange mechanisms. Typically, the diffusivity of hybrid solutes in the interstitial arrangement, is significantly greater than their diffusivity in the substitutional arrangement. Under such conditions the incorporation of solute atoms can occur by fast diffusion of interstitial and subsequent change-over to substitutional sites, as shown in Figure 3.

Frank and Turnbull[32] originally suggested this mechanism to explain the fast diffusion of copper within germanium when the change-over involves vacancies. Subsequently, the diffusion of various foreign metallic elements in polyvalent metals like lead, titanium, and zirconium was also linked to this mechanism.

The rapid diffusion of gold (Au) in silicon was originally suggested by Gösele et al. [33,34] when the change-over involves self-interstitials. Currently, this mechanism is also associated with the diffusion of other hybrid foreign elements like platinum, zinc in silicon, and zinc in gallium arsenide.

3.3 Concerted migration

Concerted migration typically occurs when multiple ions move together as a group rather than individually. By this the ions become more mobile and can move through the solid material more easily. This phenomenon is desirable because it can enhance the overall ionic conductivity of the solid material, enabling faster ion transport and thus improving the battery performance. It has already been demonstrated that similar phenomena significantly reduce the barriers of surface reactions when concerted reaction mechanisms are considered.[35] Nevertheless, such a concerted motion of the ions is not well described with conventional

diffusion models. While a comprehensive understanding of the migration mechanism has been provided, predicting $E_a = 0.5$ eV for $Li_5La_3Ta_2O_{12}$ composition,[36] the conventional model falls short in capturing the phenomenon of superionic conduction in $Li_7La_3Zr_2O_{12}$ (E_a= 0.3 eV)[37] of same crystal framework and comparable energy landscapes.[38]

During concerted migrations, the Nernst-Einstein equation fails to uphold the approximate correlation between the tracer diffusion coefficient and the ionic conductivity. As a substitute, the charge diffusion coefficient D_σ supersedes D_{tr}, and the accurate manifestation of the Nernst-Einstein equation yields the ionic conductivity as:

$$\sigma = \frac{Z_c^2 e^2 C}{k_B T} D_\sigma. \tag{9}$$

where D_σ quantifies the diffusion behavior exhibited by the center of mass of the charge carriers, $C = \frac{N_c}{V}$ represents the concentration of charge carriers in a given volume, and $Z_c e$ signifies the magnitude of charge possessed by the carriers.

The charge diffusion coefficient, in contrast to the tracer diffusion coefficient, exhibits a direct proportionality to the ionic conductivity. The literature commonly denotes the ratio between the tracer and charge diffusion coefficients as the Haven ratio $H_r = \frac{D_{tr}}{D_\sigma}$. The reduction of the effective degrees of freedom due to the cooperativity of the Li ions exhibits a direct correlation with the Haven ratio, a widely recognized metric for elucidating the cooperative phenomena observed in ion conductors pertaining to ion dynamics.[39] The examination of the inequality[40] yielded valuable empirical knowledge regarding the distinction between the tracer and charge diffusion coefficients, resulting in hints for finding materials where the carrier-carrier interaction is long-ranged.

$$0 \leqslant D_\sigma \leqslant N_{eff} D_{tr}. \tag{10}$$

In Eq. 10 N_{eff} is an effective number of particles with that the carrier can interact in a given correlation time. Note that the correlations giving a large N_{eff} have a significant impact

on the attempt frequency, assuming Arrhenius kinetics. However, these correlations do not influence the energy barriers involved in the process. This highlights the improvement of the conductivity with the factors governing the attempt frequency[40] rather than the energy barriers in the given system.

In addition, collective modes can emerge in a system of ions moving within a single-particle potential energy surface.[41] When strong ion-ion interactions constrain the ions to be spaced apart in a manner inconsistent with the energy landscape, a smoother energy landscape is experienced by the group as a whole as not all moving ions can be at equivalent extrema of the potential energy surface at the same time. These collective modes, if formed and mobile, dominate transport statistically over individual ion hops due to their higher barriers. To achieve fast ion conduction, it is important to engineer a high intrinsic concentration of mobile carriers by inducing frustration, which breaks symmetries and maximizes geometric frustration in the sublattice. Frustration flattens the energy landscape, preventing the trapping of mobile carriers in deep energy minima and promoting exploration of degenerate states within a narrow energy window, resulting in a high concentration of mobile charge carriers and high interstate transition rates.

The superionic conductivity of a variety of Li and Na solid electrolyte materials was therefore attributed to the concerted migration of charge carriers.[43,44] For example, a significant degree of cooperative charge carrier motion characterized by low Haven ratios H_r was identified in superionic conductors $Li_{10}GeP_2S_{12}$ ($H_r = 0.42$)[40] and $Na_{10}GeP_2S_{12}$ ($H_r = 0.56$).[45] In a related study the superionic conductors $Li_{10}GeP_2S_{12}$, $Li_7La_3Zr_2O_{12}$ and $Li_{1.3}Al_0.3Ti_{1.7}(PO_4)_3$ were shown to exhibit concerted migration of Li^+ based on AIMD simulations and the van Hove correlation function,[42] as shown in Figure 4. Moreover, promoting the occupation of high-energy sites in the structure was suggested to activate concerted migration. Based on a classical diffusion model and nudged elastic band (NEB) calculations it was shown that diffusion barriers for the concerted migration of several Li^+ were significantly reduced as opposed to the energy landscape for single-ion migration, constituting a design principle for

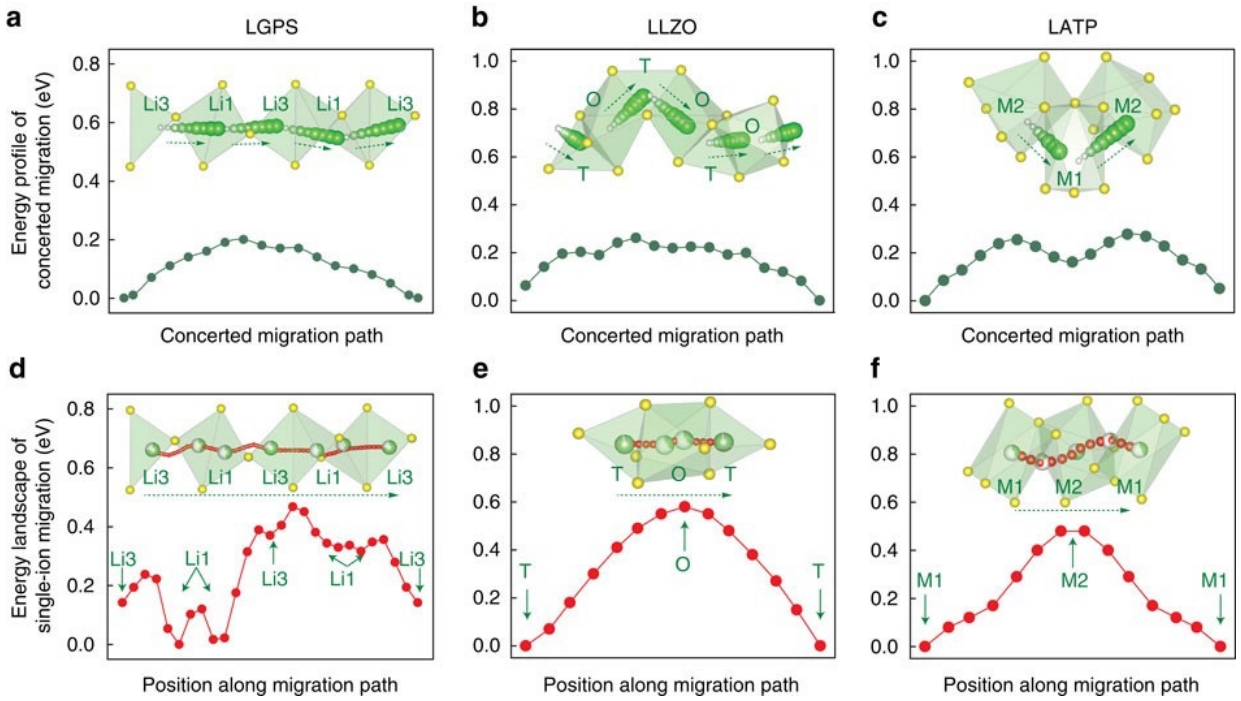

Figure 4: Energy barriers for collective migration of multiple Li ions in (a) $Li_{10}GeP_2S_{12}$ (LGPS), (b) $Li_7La_3Zr_2O_{12}$ (LLZO), and (c) $Li_{1.3}Al_{0.3}Ti_{1.7}(PO_4)_3$ (LATP), as they hop into adjacent sites along the diffusion channel. Insets depict the pathway of Li^+ ions (represented by green spheres) and the surrounding O/S ions (represented by yellow spheres). (d–f) Energy landscape of a single Li^+ ion hopping along the migration channel (shown in the insets) spanning multiple Li sites (partially filled green sphere) and the pathway of Li^+ ions (depicted as red spheres). Figure is taken from [42] with permission from Springer Nature.

novel superionic conductors. This was verified experimentally for a series of $Li_{6+x}Sb_{1-x}S_5I$ (M=Si, Ge, Sn) solid solutions in which partial substitution of Si^{4+} in Sb^{5+} sites and Li^+ in the lattice lead to the population of high-energy interstitial sites.[46] The resulting disordered Li^+ distribution was found to activate concerted migration and lead to reduced activation barriers. Hence, $Li_{6.6}Si_{0.6}Sb_{0.4}S_5I$ was identified exhibiting superionic conductivity of 14.8 $mS{\cdot}cm^{-1}$ and a low activation barrier of 0.25 eV. Concerted migration mechanisms are not only limited to Li and Na conductors. Even for multivalent charge carriers, concerted migration can lead to increased ionic conductivity as recently illustrated in $Ca_{1.5}Ba_{0.5}Si_5O_3N_6$.[47] In this material, static vacancy configurations were found to enable 1D diffusion pathways leading to temporary occupation of nearest-neighbor Ca sites. In these Ca configurations, significant interactions of mobile ions resulted in the activation of a "vacancy-adjacent"

concerted migration mechanism.

3.4 Charge analysis

The term "ion mobility" suggests that ions are moving through the host material. However, the question arises whether really ions move as there is no unique way to associate charge to a particular atom in an extended material. Consequently, partial charges are typically associated with the single atoms. While the concept of partial charges is frequently used in chemistry to gain an understanding of processes and reactions, an accurate quantum mechanical description, in the sense of a single observable, of atoms in molecules, is not possible. As a consequence, atomic partial charges have been described as "unicorns" before,[48] while Cho et al. [49] recently suggested the term "proxy variable" to be more appropriate. Regardless of the correct terminology, "atoms in molecules" (AIM) as a concept remains a somewhat arbitrarily human-defined tool. Nevertheless, many well-established mechanisms, like nucleophilic and electrophilic attacks in reactions, atomic electronegativities, or oxidation states in metalloorganic compounds, rely on this idea of an existing charge partition. There is, therefore, a substantial demand for charge partition schemes to allow QM calculations to establish a proper connection to these concepts. All such methods must divide and allocate the existing charges to their respective atoms. This division can be done in two ways: by a sharp separation of real space where every atom is allocating a specific volume or by a softer partitioning where atomic volumes can overlap. It is essential to highlight that neither of the two approaches is necessarily better than the other, and their usefulness relies heavily on the desired purpose. Many reviews, in particular within the molecular chemistry community, have addressed and discussed the variety of charge partitioning schemes available today.[50] While a comprehensive overview of the many different methods is far beyond the scope of this paper, we nonetheless wish to introduce some of the most common schemes with a focus on their implementations within the field of ion mobility in crystalline battery materials.

The Bader charge analysis method is among the most used charge partition schemes and

falls into the first sharp real space division category. Using Bader et al.'s[51] pioneer work, which establishes a quantum theory of atoms in molecules, this scheme analyses the charge density and divides the real space along minima in the charge density. Bader charges are used to partition the electron density within many material classes of particular interest for the development of batteries. In the case of Spinels, the Bader charge analysis is frequently used to derive values for the oxidation states within the material.[52–55] The importance of the oxidation state with respect to the ion mobility has been shown for both perovskites,[56] as well as layered oxides,[57] where structures with increased ion mobility can be stabilized depending on the oxidation state of the transition metal. Pramanik et al. [58] used Bader charges to highlight the importance of the oxalate group in redox processes in their perovskite oxalate material. He et al. [59] utilized the Bader charge analysis to describe the lithium mobility in layered oxides. Sotoudeh et al. [3] introduced a new descriptor concept for the ion mobility in crystalline solids in which the charge carriers charge plays an important role. This concept was derived after they had previously shown, using Bader charge analysis, that the stability of ions in chalcogenide spinels can only be understood if deviations from a purely ionic interaction are taken into account.[2]

A representative of the soft partitioning category is the Mulliken charge analysis.[60] Akin to the linear combination of atomic orbitals technique, a population analysis is used to divide the system's wave function into atomic orbitals, followed by a division of the atomic overlap population among the involved atoms.[60] Within Mulliken's initial method, the overlap population is divided equally. Improvements to the classical Mulliken charge analysis have been developed, among others, by Löwdin et al. (Löwdin charges) and Montgomery et al. (MBS-Mulliken), both of which address the fundamental problem of the basis set dependence of Mulliken charges. Hammouri et al. [61] used Mulliken population analysis to show that the lower partial charge of titanium in their spinel improves the Mg mobility. In contrast, Yu et al. [62] used Mulliken charges to investigate the electronic conductivity at the interfaces of layered oxides and spinels.

Another member of the second category of partitioning schemes is the Hirshfeld method and its many variants.[63] The Hirshfeld method calculates the charge density difference between the charge density of the system and the non-interacting atomic charge densities. Then it divides the resulting deformation density via a sharing function based on the atom's local contribution to the non-interacting atomic charge density. This distribution of the combined deformation density along a sharing function has earned the Hirshfeld method the nickname "stockholder" partition analysis. Xu et al. [64] used this method to show the influence of the anion charge on Li mobility within iodite-type compounds.

Closely related to the Hirshfeld method is the Voronoi deformation density,[65] where instead of weighing the deformation density via a sharing function, the deformation density is divided into the real space partitioning non-overlapping Voronoi cells, placing the method in the first category of charge partitioning schemes defined above.

While the different charge partition schemes tend to agree qualitatively,[66] the exact values may differ significantly. Ullah et al.[67] used multiple charge partition schemes to analyze the adsorption and mobility of alkali-ions on boron-arsenide and found values for lithium from +0.99e(Bader) to +0.18e(Mulliken). These discrepancies between the different methods are not surprising, as both Mulliken and Hirshfeld charges tend to underestimate charges,[68] while Bader charges are sometimes overestimated.[69] The choice of the charge partitioning scheme should therefore depend on the desired chemical property and an understanding of the system in question. Löwdin population analysis has been shown to yield chemically reasonable charges for a variety of Li and Na-based cathode materials,[70] while Bader charges can be used to derive oxidation states.[71] Lastly, the Hirshfeld method's use of the deformation density leads to generally physically meaningful results for the charge transfer.[65] The exact value extracted from charge partitioning schemes should, however, always be handled with caution, and any comparison between charges determined by different methods should only be attempted with a solid understanding of the methodologies of the different schemes. These difficulties concerning comparing differently derived charges may complicate future machine

learning attempts to find possible descriptors. These same discrepancies between the charge partitioning schemes make it difficult to identify the nature of the migrating charge carrier with regard to its ionicity. In order to resolve this question the charge of the migrating species in the transition state should be examined for a variety of compounds, where the Hirshfeld method is expected to yield the most reasonable results due to it deriving charges based on the deformation density.

4 Accelerated materials discovery

4.1 General remarks

Efficient ionic conductivity is a crucial factor for the development of high-performance batteries. In the pursuit of discovering materials with superior ionic conductivity, researchers are employing a combination of cutting-edge computational techniques and automated experimental investigations. This concerted approach aims to uncover new compounds and explore alternative structural configurations that can support the swift movement of ions.

One promising avenue for materials discovery lies in the utilization of high-throughput computational techniques. By leveraging the power of computational modeling and simulations, scientists can rapidly screen a vast array of potential compounds and identify those with desirable properties for ionic conductivity. This computational exploration provides valuable insights into the trends that govern ion mobility and helps to narrow down the list of candidate materials for further experimental validation.

The collaboration between computational and experimental studies is essential for verifying the predicted properties of candidate compounds. Experiments involving synthesis, characterization, and testing enable researchers to assess the actual performance of predicted materials and validate their ionic conductivity. This process allows for iterative refinement of computational models, leading to increasingly accurate predictions and a deeper understanding of the underlying principles governing ionic conduction.

In addition to modifying existing electrode materials that have shown promise in liquid-based batteries, researchers are actively exploring novel electrode materials and protective coatings tailored for solid-state battery applications. These materials must meet the stringent requirements of solid-state systems, including low and isotropic volumetric expansion during cycling.

By seeking electrode materials that exhibit low and isotropic volumetric expansion upon cycling, researchers aim to address one of the key challenges in solid-state battery technology. This feature allows for improved cycling stability and avoids the formation of cracks or delamination at the electrode-electrolyte interfaces. Consequently, the overall ionic conductivity of the battery system is enhanced, leading to superior performance in terms of energy density, lifespan, and safety.

Ultimately, the field of materials discovery for enhanced ionic conductivity is a dynamic and interdisciplinary area of research. By combining computational approaches with experimental investigations, scientists are continuously striving to identify new compounds and structural types that support fast ion conduction. Through exploring novel electrode materials and protective coatings, researchers are working towards the development of solid-state batteries with exceptional performance characteristics, bringing us closer to the realization of advanced energy storage technologies.

4.2 Descriptors and design principles

A highly valuable concept for expediting the process of discovering new materials relies on descriptors, as for example addressed by Ghiringelli et al.[72] and Isayev et al.[73] These descriptors encompass essential properties of materials or their combinations, which exhibit a correlation with the desired or undesired functionalities of the materials. This concept has demonstrated remarkable success in the field of heterogeneous catalysis, particularly in conjunction with scaling relations, as discussed by Nørskov et al.[74] and Man et al.,[75] and has already found applications in battery research, as indicated by Jaeckle et al.[76] The iden-

tification of descriptors can significantly expedite the search for novel materials possessing the desired functional properties. Once identified, these descriptors can be optimized in the initial stages of the search for materials with improved properties, allowing the identification of promising candidate materials whose properties can be thoroughly examined.

With respect to solid-state ion mobility, several potential descriptors have been suggested, such as lattice volume and ionic size,[1,30] the selection of the anion sublattice,[1,77] lattice dynamics,[1,78,79] and the preferred crystal insertion site.[80] However, many of these identified descriptors are limited to specific crystal structures, and some rely on properties that are not easily accessible.

In 2022, Sotoudeh et al.[3] conducted first-principles electronic structure calculations to develop a descriptor for ion mobility in battery electrodes and solid electrolytes. This descriptor is composed of easily accessible observables, namely ionic radii, oxidation states, and Pauling electronegativities of the species involved. The study reveals that within a specific class of materials, the migration barriers can be related to this descriptor through linear scaling relations, as shown in Figure 5. These relations can be established by varying either the cation chemistry of the charge carriers or the anion chemistry of the host lattice. The existence of these scaling relations suggests that a purely ionic perspective is insufficient for understanding all the factors that influence the ion mobility in solid materials. The discovery of these scaling relations has significant implications as it shows the potential to accelerate the process of finding materials with desired ion mobility properties such as oxide spinels.[81] By utilizing this approach, researchers can more efficiently explore and identify materials that exhibit enhanced ion mobility, thus contributing to the development of improved electrochemical devices, including batteries and solid electrolytes.

In further studies, Machine learning (ML) was employed to measure the significance of various chemical, physical, and structural characteristics on the movement of ions within a crystalline lattice.[82] This work focused on the anti-perovskite crystal structure as a model system. Multiple ML algorithms were trained to predict ion migration barriers, using a

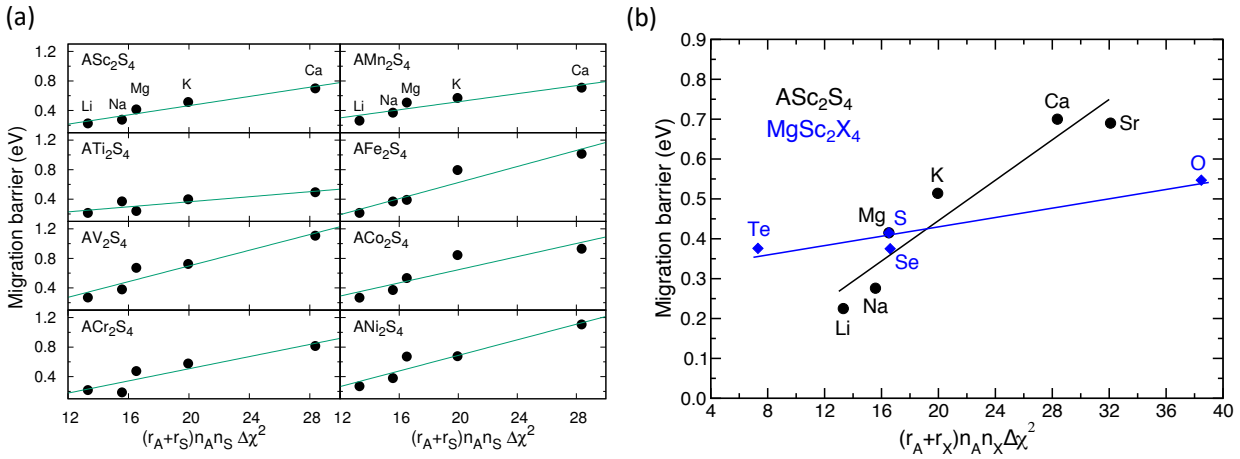

Figure 5: Migration barriers (in eV) in AB_2S_4 spinels plotted as a function of the migration number N_{migr} for (a) eight transition metal cations B = Sc, Ti, V, Cr, Mn, Fe, Co, Ni, while considering various migrating cations A = Mg, Na, K, Mg, Ca, and (b) for ASc_2S_4 (represented by black symbols) and $MgSc_2X_4$ spinels (represented by blue symbols), including different monovalent and multivalent cations (A^{n+}) and anions (X^{n-}). Reprinted with permission from Ref.,[3] published under a CC BY license.

dataset of over 600 barriers calculated consistently through density functional theory. The training set included 36 alkali metal chalco-halide anti-perovskites, encompassing vacancy and interstitial migration mechanisms (see Figure 6). Redundant features were identified and removed from the analysis to simplify the models and prevent overfitting. The most accurate algorithm was used to determine the feature combinations that yielded the most precise predictions. The study quantified the relative importance of features and their influence on ion transport using mean decrease in impurity (MDI) and individual conditional expectation (ICE) plots.

This analysis reaffirmed the significance of known mobility-influencing features, such as anion polarizability, and revealed the importance of other lesser-known factors. Notably, lattice properties like hopping distance and channel width were found to have the greatest impact on cation mobility. These features accounted for 70% of the feature importance in vacancy migration and for approximately 50% in interstitial migration, as illustrated in Figure 7. Analysis of these features using individual conditional expectation showed that barriers decrease as hopping distance decreases and channel width increases. Additional no-

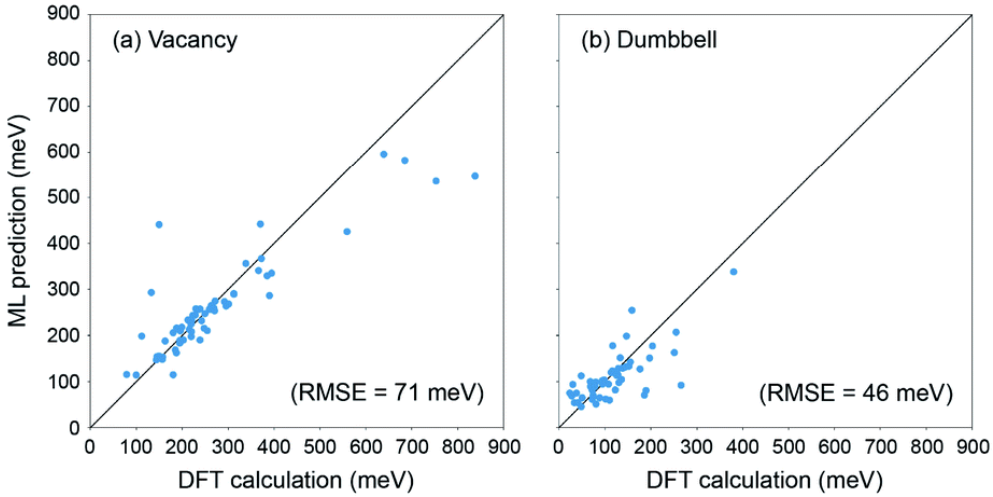

Figure 6: Comparing the effectiveness of the adaboost + ERTR ML model with DFT calculations, based on the best feature sets. (a) Predicted vacancy migration barriers using five features, and (b) Predicted dumbbell migration barriers using three features. Reprinted with permission from Ref.[82] Copyright 2012 Royal Society of Chemistry.

table features included anion polarizability (22% for vacancy migration) and defect formation energy (35% for interstitial migration). The discovery of the defect formation energy as a significant feature for interstitial migration is noteworthy as it reflects a kind of Brønsted-Evans-Polanyi-type relation between activation energies and site preference of the charge carriers.[4]

Overall, these analyses will aid in designing efficient electrodes and solid electrolytes by narrowing down the essential properties in a multidimensional design space. However, to extend the results beyond anti-perovskites, further research is necessary, such as incorporating dynamic phenomena like lattice vibrations and poly-anion rotations into the feature set. It is worth noting that the features used in this study for anti-perovskites can be readily evaluated for other types of crystalline conductors. Additionally, several important features identified here for vacancy migration have been discussed in literature for other crystal systems, indicating a potential transferability of these findings.

The olivine-type $LiMXO_4$ chemical search space was effectively screened using the DFT+NN method.[83] The multi-output node architecture (diffusion barrier and cohesive energy) proved

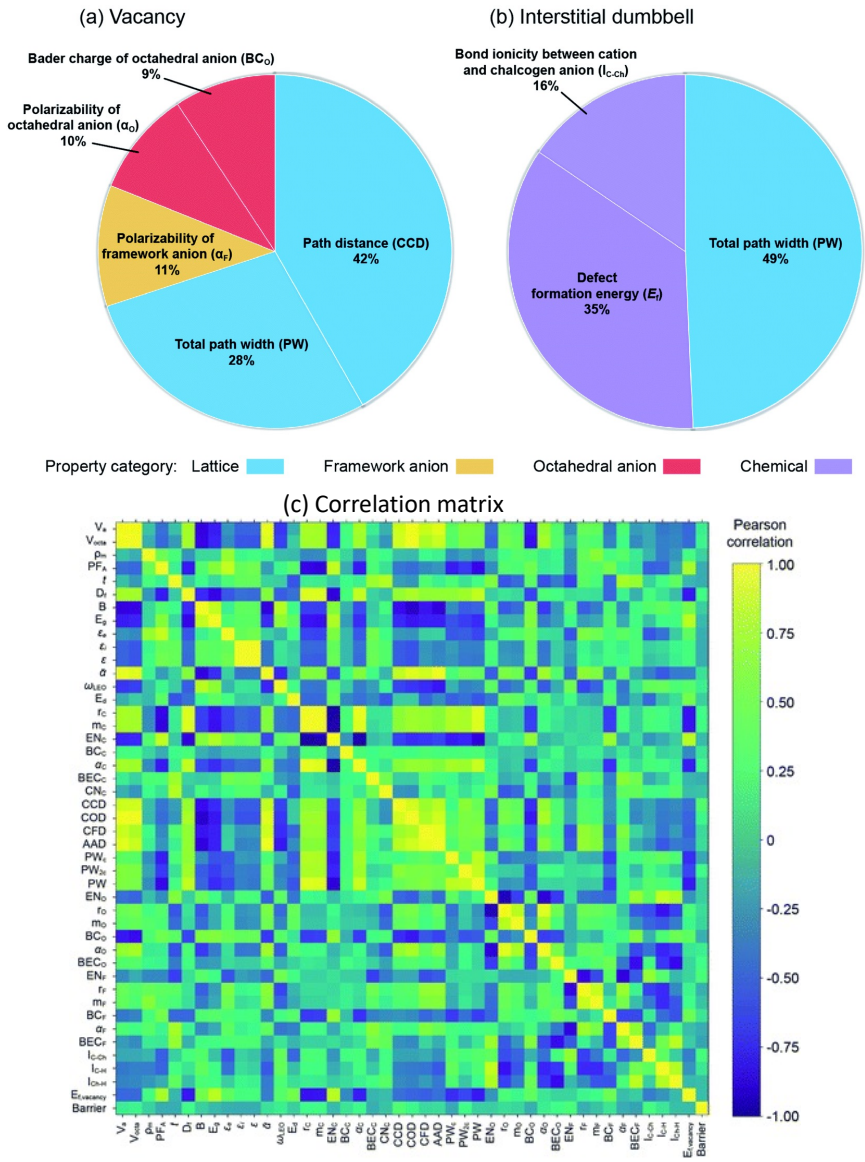

Figure 7: Assessing feature importance in ML models for ion migration through (a) vacancy and (b) interstitial mechanisms. Importance was measured using the mean decrease in impurity. (c) The correlation between descriptors and vacancy migration barriers through Pearson correlation analysis. Reprinted with permission from Ref.[82] Copyright 2012 Royal Society of Chemistry.

to be more accurate and interpretable compared to the single output node architecture and the partial least squares (PLS) based method. Significantly improved predictions were observed for values near the extreme terminals of the attribute set (diffusion barrier and cohesive energy) compared to PLS-derived models. Incorporating a penalty term on the error

function greatly reduced overfitting of the training data, resulting in a more robust model. Furthermore, utilizing literature-based multivariate input data showed promise for predicting target properties. The DFT data-based model (DN3) discovered candidate compositions such as $LiMgPO_4$ (0.26 eV), $LiMgAsO_4$ (0.17 eV), $LiScSiO_4$ (0.29 eV), and several others, including compositions containing rare earth elements that were previously unidentified. The causal index (CI) sensitivity, and variable importance in projection plots established the input-output relationships and relevance of input variables. For the DN3 model, descriptors of the local environment for the Li pass were found to be important input variables, whereas for the literature data-based neural network model, descriptors for the X cation played a crucial role. Techniques like CI plots and sensitivity profiles provided a systematic and unbiased way to interpret the models' underlying structure, but chemical reasoning is necessary to validate the input variables' relevance and identify potential issues arising from multicollinearity.

Jalen and colleagues[84] successfully developed an efficient and informative neural network-based functional for the composition space of tavorite $LiMTO_4F$, providing insights into the materials' magneto-electric (ME) properties. Among the potential solid electrolytes with ME values less than or equal to 0.30 eV, there are $LiGaPO_4F$ (0.25 eV), $LiGdPO_4F$ (0.30 eV), $LiDyPO_4F$ (0.30 eV), $LiMgSO_4F$ (0.21 eV), and $LiMgSeO_4F$ (0.11 eV). By employing an informatics-based model along with chemical intuition, this approach helps to unravel the complex interplay of various parameters that influence the desired property, often in competition with each other. Key factors such as the size of the Li pathway bottleneck, polyanion covalency, and local lattice distortion were identified. Additionally, the study demonstrated the capability of predicting the target property (e.g., ME) for multiple structure types primarily using intrapolyhedron parameters.

Another model was developed to identify the parameters responsible for high Li-ion conductivity in garnet-structured oxides.[85] These parameters, mostly based on geometry, were derived from the relationships between constituent element radii and ion packing princi-

ples. The Li ion transport characteristics in garnet-structured oxides were analyzed using regression analysis (support vector regression - SVR), revealing the relationships between composition, structure, and ionic conductivity. Promising compositions were identified using t-stochastic triplet embedding (t-STE), a method related to chemography or cartography in computer-aided molecular design. The models achieved a reasonable level of predictive ability, with the statistical parameters R-squared (R2), Root Mean Squared Error (RMSE), and Mean Absolute Error (MAE) of the SVR model reaching 0.778, 0.372, and 0.283, respectively. The predictive errors were comparable to the variances in total conductivities reported in different publications. However, there are limitations to the models predictive ability, which could be attributed to descriptor selection or intrinsic variance in the experimental data. The t-STE models demonstrated a clear allocation of chemical space areas based on the logarithm of total ionic conductivity (log σ_{tot}) values of compounds, confirming the suitability of the chosen descriptors for understanding composition-structure-property relationships. These models were used to evaluate log σ_{tot} values for candidate compounds recommended for synthesis. Attempts were made to elucidate the relative site preferences of Al^{3+} and Ga^{3+} cations, focusing on compounds potentially unstable to moisture due to the accommodation of Li^{+} in tetrahedral and octahedral sites. However, the obtained results were inconclusive. Several candidate compounds have been recommended for synthesis as potential solid-state electrolyte materials.

Introducing a novel computational screening approach, Sendek et al.[86] presented a method for identifying potential solid state electrolyte materials for lithium-ion batteries. This approach allows to screen all known lithium-containing solids, tackling the challenge of simultaneously satisfying multiple requirements for high-performance electrolytes, which is challenging to achieve through experiments or computationally intensive *ab-initio* methods. Initially, they screened 12,831 crystalline solids with lithium content to identify structures possessing high structural and chemical stability, as well as low electronic conductivity and cost. Subsequently, they developed a data-driven model utilizing logistic regression to clas-

sify ionic conductivity, based on experimental measurements reported in literature, thereby identifying candidate structures with fast lithium conduction. By employing this screening process, they narrowed down the list of candidates from 12,831 to 21 structures that exhibit promise as electrolytes, with only a few having undergone experimental examination. Interestingly, they found that individual atomistic descriptor functions lack predictive power for ionic conductivity; however, employing a multi-descriptor model proves to be useful. Furthermore, they observed that screening for structural stability, chemical stability, low electronic conductivity, and high ionic conductivity eliminates a significant portion of lithium-containing materials, reducing the list substantially. Notably, their screening approach capitalizes on structures and electronic information available in the Materials Project database. The examples presented in this chapter demonstrate that accelerated materials discovery methods are increasingly used to derive trends in ion mobility. However, it is still not clear how general the observed trends are with respect to different materials classes which will be discussed in the next section.

5 Materials classes

In the following sections we want to explore todays most important material classes of crystalline solids, which are researched for their use in battery technology. Still, the aim of this review is not a full account on all material classes since unfortunately, covering all of them is far beyond the scope of this review. Therefore, we limited ourselves to the materials classes of spinels, olivines, Garnets, perovskites, Prussion blue, Chevrel phase, layered oxides, NASICONs and anion migration systems. We are aware of the plethora of other materials out there, such as post-spinels[87], Weberites[88], Zircons,[89] Borates[90], V_2O_5[91] and $\alpha-MoO_3$[92,93].

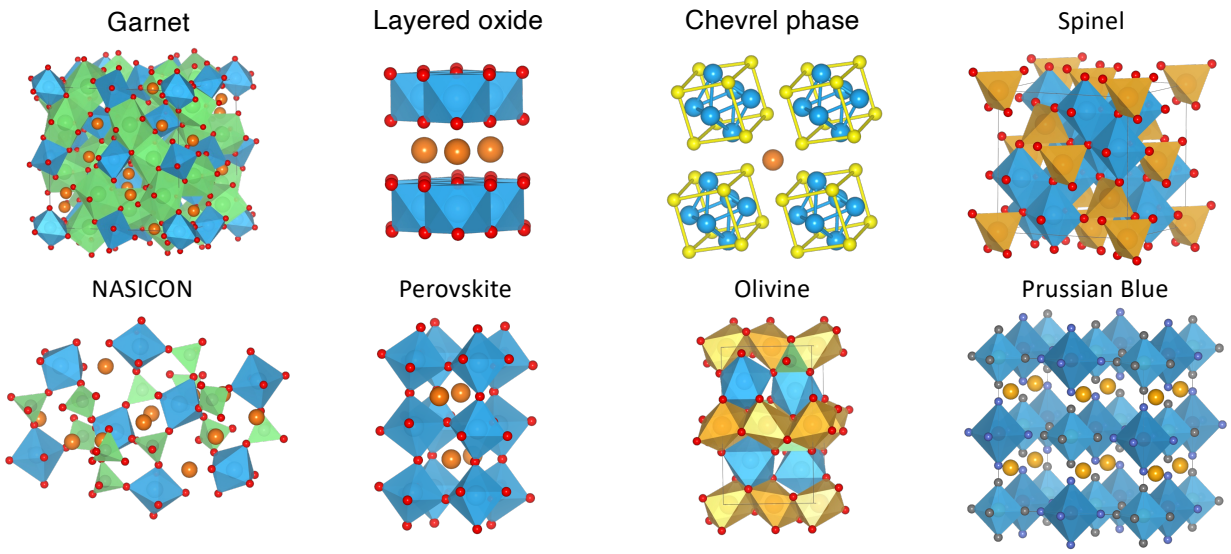

Figure 8: Supercells featuring the various crystal structures of materials considered in this study. The migrating ions are depicted with orange spheres or polyhedra, while the transition-metal ions are represented by blue octahedra. Green polyhedra symbolize the presence of polyanionic groups.

5.1 Spinels

The spinel structure with a general formula AB_2X_4 consists of a cubic close-packed arrangement of X atoms. In its conventional crystal structure, the A cations occupy 1/8 of the tetrahedral sites, while the B cations occupy 1/2 of the octahedral sites, as depicted in Figure 8. The B and X ions create a network of BO_6 octahedra that share edges, while the A and O ions form a three-dimensional network of tetrahedra that share corners. The A-type ions are relatively small, making their occupancy of the tetrahedral sites energetically more favorable than the occupation of the octahedral sites. The pyrochlore lattice is formed by the B ions, typically leading to pronounced geometric frustration effects. Along the [111] direction, two types of alternating stacking planes can be observed: a two-dimensional triangular lattice and a kagomé lattice. The A sublattice of the spinel structure assumes a diamond lattice shape. The presence of various competing factors, such as the crystal field stabilization of the transition metals (B cations) or entropic contributions, can give rise to a range of disordered or inverted configurations. In certain cases, a fraction of A cations, such

as Mg, can swap places with the transition metal B cations, resulting in partially inverted lattices and charge disproportionation of the B cations ($2B^{3+} \rightarrow B^{2+} + B^{4+}$).

At high temperatures, numerous spinels exhibit cubic symmetry; however, the presence of distorted BO_6 octahedra cannot be dismissed. The octahedra undergo a trigonal distortion, leading to a transformation from O_h octahedral symmetry to D_{3h} octahedral symmetry.[2,81]

Li-ion batteries have effectively incorporated Mn_2O_4 spinels into commercial applications as cathodes. Nevertheless, this specific spinel exhibits a significant obstacle to Mg^{2+} diffusion, with a barrier of 0.67 eV. This value surpasses the migration barriers for Li^+ ions in all M_2O_4 spinels (where M = Mn, Co, Ni, Cr), which range from 0.40 to 0.60 eV.

The spinel structure possesses a desirable combination of capacity and voltage.[81] Recent studies[94,95] have reported experimental migration barriers of approximately 600 meV for Mg^{2+} in Cr- and Mn-spinel oxides, aligning with density functional theory (DFT) calculations. It has been observed that structural disorder within the spinel lattice affects the migration of Mg ions, and this disorder can be regulated during synthesis. Nonetheless, the strong Coulombic interactions between the Mg cations and the oxide host lattice generally impede the reversibility of Mg intercalation and result in elevated Mg migration barriers. In addition, migration in the spinel structure is mediated by intermediate octahedral sites whose relative stability to the initial tetrahedral site, called site preference, strongly influences the resulting migration barriers.[80] In the ideal scenario in which the site preference tends towards zero, the activation barriers minimize and any deviations towards higher or lower values result in an increased barrier. This observation can be inferred from the relationship between the activation barrier and the site preference, as depicted in Figure 9. As a result, this phenomenon presents potential avenues for augmenting charge carrier mobility through deliberate choices of B-group transition metals and anion chemistry that satisfy the site preference criterion. Such improvements are evident in the low migration barriers of Ca in d_0-metal oxide spinels.[4] Migration barriers in spinel materials have recently been used to derive a descriptor for the ion mobility based on ionic radii, oxidation states, and

electronegativities, as mentioned in the previous section.[3] Additionally, it was shown that transport properties of spinel compounds are impacted by transition metal cations, discovering that these metals have a notable impact on the barriers for Mg^{2+} migration in such compounds.[2,81] By utilizing this principle, it was demonstrated that oxide spinels incorporating electronegative transition metal cations of substantial size hold the potential for showcasing elevated Mg^{2+} mobility.[81]

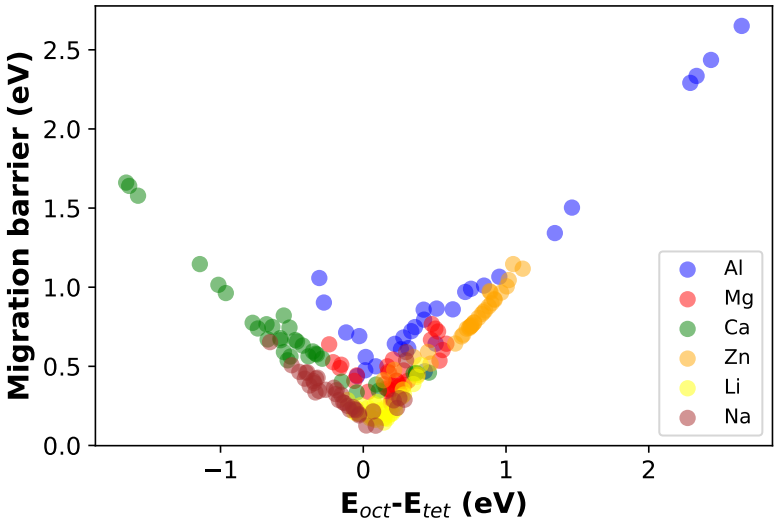

Figure 9: The migration barriers obtained from NEB calculations against the site preference $E_{oct} - E_{tet}$ for various spinel compounds: Al (blue), Mg (red), Ca (green), Zn (orange), Li (yellow), and Na-based (brown) materials. Data are obtained and replotted from Refs.[4,22]

Sulfide and selenide spinels have garnered attention due to their potential as solid electrolytes in solid-state batteries. Among these compounds, $MgSc_2Se_4$ has emerged as a promising contender with a remarkably low migration barrier of $E_a = 0.37$ eV.[2,28–30] Nevertheless, its suitability as a solid electrolyte is impeded by a significant partial electronic conductivity. Moreover, studies have indicated that the mobility of magnesium in chalcogenide spinels that include lanthanoids escalates proportionally with the lanthanoid's size.[22,29]

5.2 Olivines

The utilization of an olivine structured material as positive electrode material was pioneered by the group of Goodenough in 1974.[96] This material class exhibits the general formula of $AMXO_4$, the A site mostly being occupied by Li, although the intercalation of other alkali metal ions has been studied as well.[97,98] The transition metal site is most popularily occupied by Fe, Mn, Co or Ni, while X typically equals P, less often Si or Ge.[96] From a geometric point of view, the olivine structure consists of MO_6 octahedra, that are connected to two LiO_6 octahedra and one XO_4 tetrahedra via shared edges.[99] Its crystal structure is depicted in Figure 8.

Early studies on the diffusion of charge carrier species within olivine materials assumed a strictly 1D diffusion material, consisting of channels that permeate the whole crystal system in the [010] direction.[100] However, new measurements indicated a de facto 2D migration of lithium ions in the olivine structure,[101] which contradicted theoretical studies during that time that claimed the cross-channel migration to be significantly unfavored.[102] Further theoretical studies could then reveal the possibility of cross-channel diffusion, initialized by the formation of either a Li^+/Fe^{2+} antisite defect or a Frenkel defect of an Fe^{2+} ion in $LiFePO_4$.[103,104] This cross-channel diffusion was then found to contribute significantly to the overall migration, even at low defect concentrations.[104] Subsequently, Yang et al. could observe the cross-channel migration of lithium atoms upon the formation of antisite defects in their ab-inito molecular dynamics simulations.[105] Furthermore, they determined the cross-channel diffusion to be competitive with the in-channel diffusion, finding a theoretical verification for the experimentally observed 2D migration. Therefore, while bocking diffusion in the [010]-direction, these defects open up alternative channels for the lithium ion migration.[106] Most of the published results on the diffusion coefficient for lithium ion diffusion within olivine structured materials ranges from 10^{-11} to 10^{-15} cm^2 s^{-1}.[107] Theoretical works find energy barriers of around 0.35 - 0.4 eV, overestimating experimentally found diffusion coefficients.[108] These differences may be pinpointed to many factors, including the

assumed uni-lateral nature of lithium ion diffusion in many theoretical works and the two phase coexistence / phase transformation during experiments.[102,109]

Olivine materials are especially interesting as energy storage materials due to their high operating potentials and high capacity, but the scientific interest in the optimization of olivine structured compounds increased even further with the recent successful commercialization of $LiFePO_4$.[110] Most of today's research focuses on either ridding this popular system from its known drawbacks, i.e. their low energy density and slow rate performance or on the development of its derivative systems utilizing manganese, cobalt or nickel.[111,112]

5.3 Garnets

The utilization of the strategy to replace Li^+ ions with ions carrying greater positive charges, thereby creating vacancies through which lithium ions can migrate, has been proven effective for materials exhibiting crystal structures akin to the mineral garnet.[36,113–115] $Ca_3Al_2Si_3O_{12}$ serves as the prototype material in this family, belonging to a group of substances known as orthosilicates, which possess isolated tetrahedral SiO_4 groups. The oxide ions are arranged in layers, adopting a slightly distorted hexagonal close packing. A brief discussion on several materials sharing this structure will present in Section 5.8. Another example featuring a related olivine structure is the popular positive electrode material $LiFePO_4$, which was addressed in Section 5.2. Within the garnet structure, the Ca^{2+}, Al^{3+}, and Si^{4+} ions exhibit 8-, 6-, and 4-fold coordination with neighboring oxide ions. It is common to find substitutions of similarly charged cations in these positions within this mineral family.

An example of a lithium-conducting solid electrolyte belonging to this group is $Li_5La_3M_2O_{12}$, with the M ion potentially being Nb or Ta. These materials were reported to possess lithium ion conductivities of approximately 10^{-6} S cm^{-1} at room temperature, which is roughly three orders of magnitude lower than the data reported for the previously mentioned $(La,Li)TiO_3$ materials.[116]

However, these materials can possess a significant advantage over the titanium-containing

counterparts, as it has been observed that the Ta-containing version maintains its white color even when in contact with molten lithium, indicating apparent stability against highly reactive lithium. This suggests that it could be utilized in cells operating at higher output voltages compared to those limited to higher potentials.

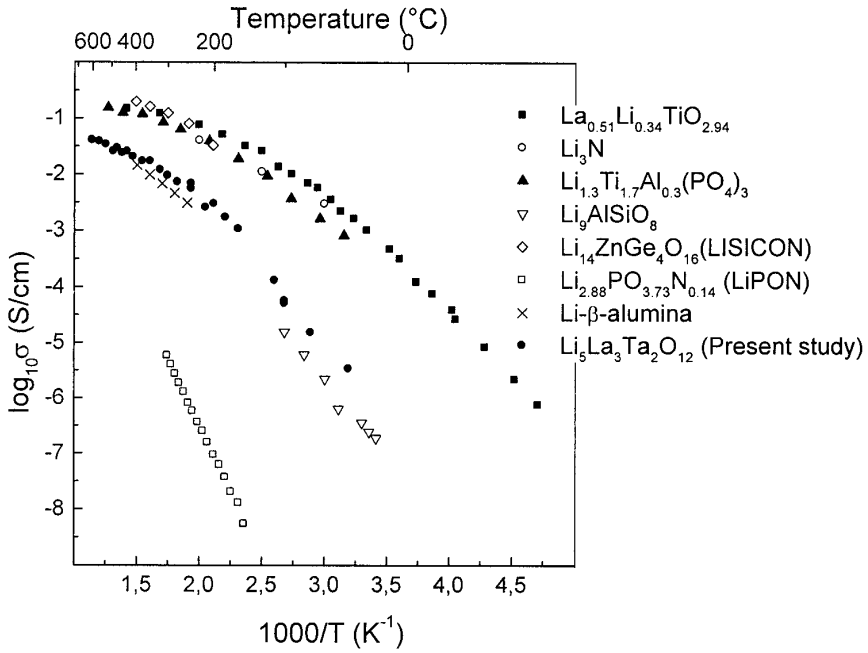

Figure 10: Exploring the total conductivity: $Li_5La_3Ta_2O_{12}$ in comparison to established lithium ion conductors. Surpassing Li-β-alumina and LiPON in conductivity, while demonstrating comparable performance to perovskite-type (Li, La)TiO_3 and Lisicon. Reprinted from Thangadurai et al. [36] With permission from The American Ceramic Society.

Figure 10 illustrates the temperature dependence of the ionic conductivity in various lithium-conducting materials.[36] The electrical conductivity activation energies for $Li_5La_3Nb_2O_{12}$ and $Li_5La_3Ta_2O_{12}$ at temperatures below 300°C are 0.43 eV and 0.56 eV, respectively. These values are comparable to those reported for the lithium ion conductor Lisicon (0.56 eV) and higher than the values for Li_3N (0.25 eV). $Li_5La_3Ta_2O_{12}$ exhibits a conductivity similar to Li-β-alumina and Li_9AlSiO_8, significantly higher than thick pellet LiPON, and slightly lower than $Li_{14}ZnGe_4O_{16}$ and $Li_{0.34}La_{0.51}TiO_{2.94}$. Further investigations have also explored the replacement of some La^{3+} ions with divalent alkaline earth ions,[113] revealing that the size of the substituted ion influences the measured ionic conductivity, with the substitution of Ba^{2+}

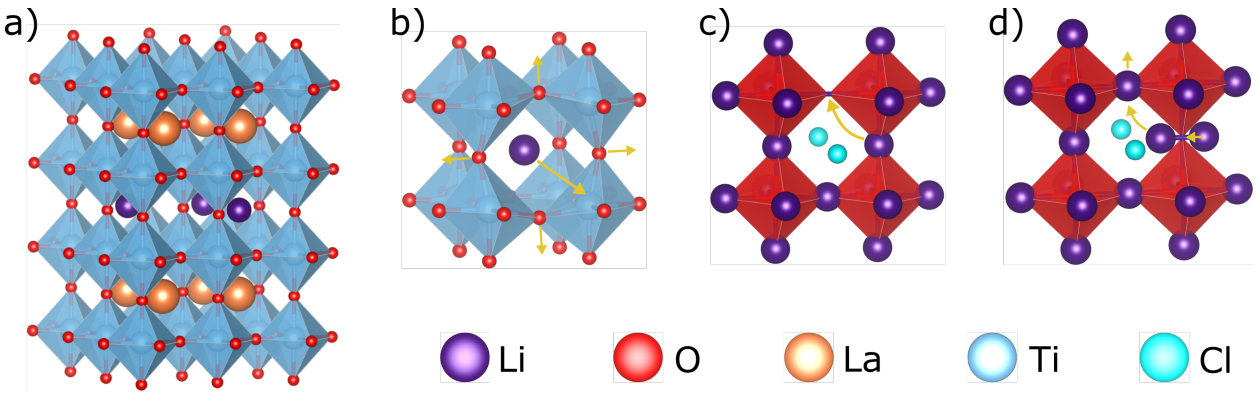

Figure 11: a) Lattice of ordered $Li_{3x}La_{2/3-x}TiO_3$ perovskite exhibitng Li-rich and La-rich layers. The vacancies are located in the Li-rich layers. b) Diffusion mechanism of Li^+ in $Li_{3x}La_{2/3-x}TiO_3$ to a vacant A-site. The oxygen rectangle represents the bottleneck which expands during the diffusion process. c) Vacancy diffusion mechanism in Li_3OCl anti-perovskite along the edge of the octahedron. d) Interstitial diffusion mechanism in Li_3OCl anti-perovskit from a dumbbell configuration to a singly occupied site where a new dumbbell will be formed.

ions yielding the highest conductivity values. Although the conductivity of the modified material, $Li_6BaLa_2M_2O_{12}$, was slightly lower than that of the original material, it encountered fewer issues with additional grain boundary impedance. Note that the impedance measurements allow to separate single crystal from grain boundary conductivity.

Furthermore, these garnet materials exhibit stability when in contact with elemental lithium, and recent findings indicate that they do not display any reactive behavior towards several frequently employed positive electrode materials.[114]

5.4 Perovskites

Perovskites are crystalline phases with the general stiochiometry ABX_3 where the cation on the B-site and the anion on the X-site form a rigid scaffold of corner sharing BX_6 octahedra. The voids between these octahedra are occupied by the potentially mobile A-species (Figures 8 and 11a). The ideal perovskite structure is cubic with spacegroup $Pm\bar{3}m$. Most perovskites, however, attain lower symmetry due to tilted/distorted octahedra and/or displacement of the cations.

Clearly, within the battery community lithium lanthanum titanate (LLTO) is the most

prominent Li^+ conductor of the perovskite family. The studies of Bezou et al.[117] and Inaguma et al.[116] are commonly referred to as the first ones reporting an A-site deficient perovskite structure for $Li_{3x}La_{2/3-x}TiO_3$ ($0.04 < x < 0.17$) and bulk ionic conductivity of $\sim 10^{-3}$ S/cm at room temperature.[118] It has been widely acknowledged[1,118] and theoretically confirmed[119] that the diffusion proceeds via a vacancy mechanism where Li^+ migrates through a bottleneck made up of four O-ions which expands in size during the diffusion process (Figure 11b). Evidently, the number of lattice-Li^+ and the number of vacancies plays a crucial role for ionic conduction, so fine tuning the parameter x has been a focus of research.[118–120] A further improvement could be achieved by widening the diffusion channel through Sr^{2+}-doping on the A-site.[121] Additionally, it has been found that depending on synthesis route and operating temperature poorly conducting La-rich layers are formed in the crystal structure constraining the Li^+ diffusion to two dimensions. This transition from the disordered to the ordered state is accompanied by a drop of one order of magnitude in conductivity.[122–125] Nevertheless, by aligning the conducting planes along the measurement direction, a value of $4 \cdot 10^{-3}$ S/cm has been recently reported for a 13 μm single crystal.[126]

Although high resistance at the grain boundaries and low stability vs. Li metal induced by Ti^{4+}/Ti^{3+} redox activity have so far prevented LLTO from application, it serves as a well studied model system for ionic diffusion in perovskites. The replacement of Ti^{4+} with Nb^{5+}, for instance, resulting in $Li_xLa_{(1-x)/3}NbO_3$ (LLNO)[127] is an obvious idea which has gained renewed interest lately. As in the case of LLTO, Sr^{2+}-doping[128] and exploiting A-site ordering[128,129] were done to improve the material's properties, however, the bulk conductivity of 10^{-4} S/cm could hardly be increased. Exchanging the shuttle ion in LLTO from Li^+ to Na^+ and Mg^{2+} was not feasible owing to the very low mobility of the respective ions in the given hosts.[124,130] Nonetheless, in the case of Na^+ switching the B-site cation from Ti^{4+} to Nb^{5+} or Zr^{4+} could drastically improve the Na^+ mobility exhibiting conductivity values of $\sim 10^{-5}$ S/cm for $Na_{0.25}La_{0.25}NbO_3$ and $Na_{1/3}La_{1/3}Sr_{1/3}ZrO_3$.[131,132]

Some promising ionic conductors of an entirely different perovskite-related material's

class have gained strong interest during the last decade: the so-called anti-perovskites. These compounds, usually denoted X_3BA, exhibit the typical perovskite structure while having the positions of the cations and the anions exchanged i.e. X is a cation whereas A and B are anionic species. The noteworthy breakthrough of anti-perovskites in battery research was achieved by Zhao and Daemen who reported Li^+ conductivities of $\sim 10^{-3}$ S/cm in $Li_3OCl_xBr_{1-x}$ (x=1, 0.5) at room temperature.[133] In contrary to ionic conduction in usual perovskites the diffusion mechanism in Li_3OCl-type materials is an ongoing subject of discussion. Two mechanisms visualized in Figure 11c and d have been suggested: (i) A vacancy mechanism where Li^+ migrates along the edges of the cation octahedra to a vacant X-position. (ii) An interstitial mechanism where two Li^+ are located in a X-site centered dumbbell configuration; the migration of one Li^+ leaves behind a singly occupied X-site to form a new dumbbell with a neighbouring Li^+.[134,135]

One recently discussed topic is the introduction of so-called superhalides (polyanions with charge -1) at the B-site of antiperovskites. Sun et al. reported the Na^+ ionic conductivity of $4.4 \cdot 10^{-3}$ S/cm at room temperature in $Na_3O(BH_4)$ which is among the highest values measured in Na^+ solid electrolytes.[136] Supported by DFT analysis the authors attributed the outstanding conductivity to the so-called paddle-wheel mechanism i.e. the ability of the anisotropic superhalide to lower the local potential for the migrating cation by rotational motion.[136,137]

5.5 Prussian blues

Prussian blue ($KFe[Fe(CN)_6]$) is a metal organic framework (MOF) - with the general formula $A_{0-2}M[M`(CN)_6]$ and space group $Fm\bar{3}m$ (225) - consisting of two types of iron atoms that are octahedrally interconnected by cyanide ligands.[138] These iron atoms can be distinguished by their spin state, either high-spin (S=5/2) or low-spin (S=0), depending on whether they are coordinated by the nitrogen or carbon site of the cyanide ligand, respectively.[139] The possibility to exchange the M and M` sites with either electrochemically active (Mn) or

inactive (Cu, Ni) transition metals adds an additional element of customizability towards the application to this material class. Furthermore, the atomic arrangement generates a spacious framework with large channels (∼1.6 Å)[140] into which a variety of cations can be intercalated into the material.[141,142]

Still, Prussian blue analogues received the high scientific interest in their application as battery material only after their drastic performance improvement in 2015, when Goodenough and coworkers reported a rhombohedral modification of Prussian blue that occurred when the interstitial water was removed from a cubic, sodium-rich Prussian blue material in a drying process.[143,144] This new kind of Prussian blue indeed shows a longer cycle life compared to the purely cubic material and a highly reversible phase transition between the modifications.[145]

The charge carriers were proposed to reside in the large body-centered voids within the Prussian blue framework since the emergence of the earliest structure model by Keggin and Miles in 1936.[138,146] Recent research on the other hand suggests that all cations independent of size try to stay in or as close to the face-centered sites as size allows and uniformly display an aversion to the body-centered void.[147,148] These suggestions are accompanied by claims that the main transport pathway throughout the cubic Prussian blue framework is not the hopping of charge carriers from body-centered void to body-centered void. Instead charge carriers prefer to move along the cyanide grid in what the authors call a ladder mechanism - always staying close to a face-centered site and revolving around an iron atom towards the next face-centered site while avoiding the body-centered voids.

The typically reported diffusion coefficients for both modifications range from 10^{-9} to 10^{-12} cm^2 s^{-1}.[149] There are a few reports that state drastically lower diffusion coefficients of 10^{-13} cm^2 s^{-1} and below. Komayko et al. showed that for nanosized materials one does not need the assumption of a fast ionic / electronic transport in the bulk lattice, as even low apparent diffusion coefficients translate into impressive rate capabilities.[149,150] They argue that Prussian blue powders easily disperse when in contact with electrolyte and that the

agglomerates are highly permeable for the electrolyte. Consequently, shortest way of diffusion during (de-)intercalation is through the primary particles instead of diffusion though interparticle grain boundaries within the agglomerate. They suggest that one should use the size of the primary particle instead of the agglomerate size for the calculation of diffusivities, which would lower the apparent diffusion coefficients by 3-5 orders of magnitude. An overview over many experimental results can be found in the account of Komayko et al.[149] Furthermore, the diffusivities of some Prussian blue analogue structures might be limited by their effective electronic conductivity within the agglomerates, instead of slow solid state diffusion rates.[151]

Reports on theoretical calculations employed for the determination of energy barriers and diffusion coefficients in the Prussian blue framework are still scarce. Peng et al. did report energy barriers of 0.38 - 0.57 eV for the diffusion of sodium in nickel and cobalt Prussian blue analogue structures.[152] Their report indicates an increase in the energy barriers by about 0.1 eV when crossing the body-centered void, further verifying it as a non-equilibrium position. Furthermore, there are the reports of Nordstrand et al. utilizing a semi-empirical tight binding approach to determine the charge carrier mobility.[147,148] They report energy barriers for diffusion events from one face centered site to another to exhibit an energy barrier of 0.32 - 0.39 eV. The diffusion through a body-centered void is comparatively unfavored, showing energy barriers of 0.69 eV. These values closely matched the accompanying experimental diffusion coefficients, determined by cyclic voltammetry and electrochemical impedance spectroscopy measurements. The values for the energy barrier are significantly increased to 1.5 eV, when considering the diffusion through the large void created by a $Fe(CN)_6$-vacancy. Baumgart et al. utilized first-principle calculations to calculate a activation energy of 0.3 eV for diffusion events in Prussian blue, which agree well with the previous reports.[153] Furthermore, they could show that the activation energies for diffusion events in the rhombohedral and cubic modification are almost identical.

5.6 Chevrel phase

The Chevrel phase (CP) is a well known material with high ion mobility. The general formula for a Chevrel phase is Mo_6T_8 (T=S, Se or Te) with sulfur being the most used cage material. In its structure a nearly cubic sulfur cage holds an octahedral molybdenum cluster forming its unique crystal structure, as depicted in Figure 8. The CP cluster structure creates cavities and channels between the blocks within the crystal lattice and are classified as 3a, 3b, and 9d according to crystallographic symmetry.[154] Sites 3a and 9d can be occupied by cations functioning as charge carriers, making them interesting candidates for potential applications in solid-state ionic conductors while sites 3b are unfavorable for cation storage due to the strong electrostatic repulsion with the face-sharing Mo atoms.[154–156] An important factor for all solid-state ionic conductors is the quick delocalization inside the material, which is directly related to cations spacing and crucial for the cation mobility. In the CP this is achieved by the two intercalation sites at 3a and 9d. The first is the so-called inner ring site, which consists of six energetically equal sites that form a highly symmetric ring around the 3a position. The 3a position lies in a cavity which is coordinated with eight sulfur atoms, each being the corner of one CP cluster. The nearly degenerate nature of these positions, with a barrier of approximately 0.1 eV,[154] makes them favorable for accommodating a single Mg cation within the CP bulk.[5] From there it can diffuse in all three lattice directions by passing through the channel 9d. About 0.5 Å away from the 9b site in the channel are the two outer ring sites.[157] Upon occupying all inner ring sites with one cation each, the outer ring sites can accommodate an additional Mg cation per CP cluster. The CP can take up to 4 electrons until its valence band is filled and the structure transforms from a metal-like material to a semiconductor, making it possible to insert up to four monovalent cations.[158] Upon intercalation of divalent Mg, the CP undergoes a two-step charge redistribution process, which is particularly fast, as X-ray photoemission spectroscopy experiments have revealed.[159] The first electron is taken up by the sulfur cage, while the second one then gets transferred on the octahedral Mo-cluster. The CP was shown by

Aurbach et al. to achieve a discharge voltage between 1 and 1.3 V, with a theoretical energy density of about 135 $Wh \cdot kg^{-1}$.[160–162] From the observed plateaus in the charge/discharge curve, Aurbach et al. already inferred the existence of two different insertion sites which could later be confirmed to be the inner and outer ring sites.

Today it is mainly used as a cathode in magnesium batteries[155,160,162,163] as well as for other multivalent charge carriers such as Zn^{2+}.[164,165] It is named after the French scientist J. R. Chevrel, who first discovered it in 1973.[155,166] Using the CP as a cathode material overcomes the challenges of sluggish Mg ion insertion on the cathode side and the low reversibility of the process, which are commonly encountered issues with multivalent ions. This is attributed to the strong bonds they typically form with most cathode materials.[167] The CPs biggest advantage over other possible cathode materials is the reversibility of the insertion of charge carriers due to the minimal structural changes upon intercalation. Most other materials bind especially multivalent ions too strongly to be deintercalated during the charging process.[167] The CP however has a metallic ground state and thus shields the charge carrier so effectively that it can easily shield divalent charges.[158]

The sulfur cage can also be substituted with selenide and tellurium, but these elements are toxic and therefore can lead to safety problems which makes them harder to handle. Many experimental studies are thus performed on the sulfur phase though research suggests that the Se phase performs with improved capacity and kinetics, even a partial substitution of $Mo_6S_{8-x}Se_x$.[163,168,169] This is because the triclinic distortion in selenide enlarges the distance between inner sites and shortens the distance between inner and outer site, thus opening possibilities for tailoring the ionic conductivity of the system.[170,171]

There are some theoretical reports on the diffusion of cations other than Mg, which showed a direct correlation between ionic radius and the diffusion barrier as a descriptor for the ion mobility in the CP specifically,[5] as illustrated in Figure 12. This has been attributed to space limitations at the narrow transition states for migration making Pauli repulsion the main factor determining the barrier heights. There are also some studies studying the

diffusion properties of Ca.[168,172] The calculations of Juran et al.[168] reach a voltage of 2.1 and 1.8 V for the respective intercalation steps of Ca using the HSE functional, which agree reasonably well with another study, which found values of 1.9 and 1.4 V for a comparable PBE functional reference calculation.[5]

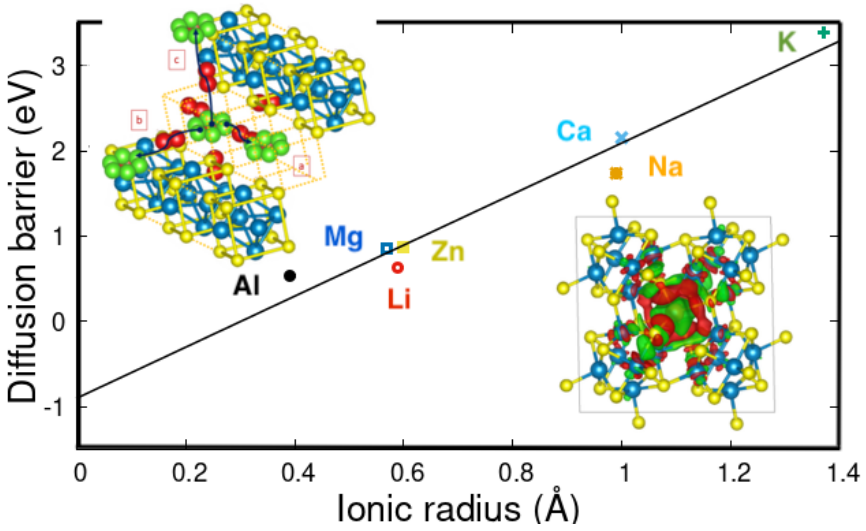

Figure 12: The correlation between ionic radius (in Å) and the diffusion barrier (in eV) for different charge carriers, using the revPBE+D3 functional. The ion mobility in the chevrel phase exhibits a significant size dependence. This size dependence is evident from the linear scaling of diffusion barriers with the ion radius of the charge carriers, regardless of their charge. It suggests a distinctive and geometry-driven diffusion mechanism within the chevrel phase. Figure is taken from.[5] The visuals are the diffusion pathways labeled as a, b, and c on top left, connecting from the inner ring position (green) within a cavity, traverse through the outer ring positions (red), and reach the adjacent cavity with the next inner ring position. While the variation in charge density illustrated in bottom right, represented regions of charge accumulation in red, and areas of charge depletion in green.

There are also numerous experimental studies addressing not only the diffusion of Mg, but also other cations such as Ca,[173] Al,[174,175] Zn,[164,165,176] Na[169] and Li.[169,177] The electronic structure and ionic diffusion properties were evaluated by phonon dispersion[156] and in another approach continuum modeling is employed to monitor the system. Usually the efficiency of the solid state system is limited by the reachable capacity, but was found by Drews et al. to be limited by the particle size of the chevrel phase material with particles smaller than $\sim$0.5 μm being crucial to avoid transport limitations for a wide range of practical current densities.[178] Another interesting field for the CP is the usage of dual ion

systems. This was investigated by Li et al., proving that the diffusion of divalent Mg ions is significantly facilitated by using a Li and Mg dual-ion system as the activation energy is remarkably reduced specifically by the concerted interactions of preceding Li ions and following Mg ions.[179]

5.7 Layered oxides

In these materials, the layers are formed by edge-sharing MO_6 octahedra, in between which the alkali ions are intercalated. The stacking of the transition metal layers forms either prismatic (P) or octahedral (O) charge carrier sites with a different number of layers in the unit cell, categorized by the Delmas notation.[180] The preferred coordination environment of the charge carriers and the stacking order depend on the nature of the charge carriers and the exact stoichiometry of the material. This is apparent when comparing the stereotypical cathode materials $LiCoO_2$ and Na_xCoO_2. $LiCoO_2$ adopts the O3 structure,[181,182] while Na_xCoO_2 can adopt either the O3, P2 or P3 structure,[183] differing in the respective oxygen stacking sequence.

In the O3 structure, diffusion can occur either via oxygen dumbbells or via tetrahedral sites when divacancy configurations are present,[184] with the divacancy mechanism exhibiting much lower barriers. In addition, the diffusion barriers were found to depend strongly on the local charge carrier configurations and thus can vary by several orders of magnitude with the charge carrier concentration.[185,186] It is noteworthy that the activation energy for the divacancy diffusion mechanism is slightly lower in $NaCoO_2$ than in $LiCoO_2$[187] illustrating the non-monotonic influence of ion size on mobility. Furthermore, the presence of larger Na^+ ions promotes the stability of prismatic sites, such as those found in P2 structures, and drastically influences ion mobility. As a result, complex trends of ion mobility with concentration are observed. In the P2 structure, the presence of two different prismatic Na sites (Na_e shares an edge with the MO_6 octahedra, while Na_f adopts a face-sharing coordination) destabilizes divacancy configurations, leading to a change in the diffusion mechanism in contrast to the

O3 structure. While the diffusion barriers are generally lower in the P2 structure, the strong electrostatic Na-Na repulsion at high Na concentration leads to high barriers and sluggish Na diffusion.[186]

The first commercially used cathode materials for Li-ion batteries TiS_2[188,189] and $LiCoO_2$ (LCO)[190] as well as many other commercial Li cathode materials such as Ni-Mn-Co-oxide (NMC) or Ni-Co-Al oxide (NCA) crystallize in a layered structure. Layered structural motifs are also currently under intense investigation not only in the context of Li-ion batteries but also in the field of post-Lithium batteries. For example, layered oxide materials with the general formula Na_xNO_2 (M=Fe, Mn, Ni, Ti, Cr or Co) are among the most promising cathode materials for Na-ion[191,192] and K-ion[193] batteries.

Moreover, layered structures were also shown to succesfully intercalate multivalent ions such as Mg in TiS_2[194] and $TiSe_2$.[195] Nevertheless, the high Mg diffusion barriers of 1 eV in TiS_2 require elevated temperatures to reversibly extract Mg from the structure. This strategy resulted in a high reversible capacity of 115 $mAhg^{-1}$ at 60°C for $MgTiS_2$,[196] however, still significant Mg entrapping in the initial cycles was found to impede the electrochemical performance. Interestingly, the mode of intercalation was found to deviate from the solid solution behavior of Li in TiS_2 and instead, Mg-vacancy orderings are found that could contribute to the observed Mg entrapping during the initial cycles.[196,197]

5.8 NASICON

Sodium (NA) Super Ion CONductor (NASICON) compounds were first researched as solid electrolyte material by Hong and Goodenough in 1976.[198,199] A decade later, they were adapted as positive and negative electrode materials as well.[200,201] NASICONs are polyanionic materials, which exhibit great structural stability and high ionic conductivity - especially for sodium ions. They belong to the family of superionic conductors, which are materials that display exceptionally high ionic conductivity at or near room temperature. Furthermore, they are classified as a polyanionic compounds, meaning they contain anions

with multiple negative charges, such as the characteristic, tetrahedral anionic units XO_4 or their derivatives.[202] The NASICON structure has the general formula of $A_xMM'(XO_4)_3$, typical elements being A = Li, Na, K, Mg, Ca and A_x = 0 - 5, M/M' = Fe, V, Ti, Zr, Mn and X = S, P, Si.[203] Depending on the elements used - and sometimes the content of sodium - the NASICON structure adopts many different crystal structures, the most common being rhombohedral, which consists of corner-sharing $M/M'O_6$ octahedra and XO_4 tetrahedra.[204] Within this crystal structure there are two distinct positions for monovalent ions, often called Na1 and Na2.[205] Both are located in an $M/M'_2(XO_4)_3$ environment - Na1 aligned along the c-axis, Na2 along the b-axis. Ions occupying the Na2 positions are the first to be extracted from the structure due to the weaker bonding caused by a longer Na-O bond lengths. The occupation of the Na2 position also leads to a significant structural rearrangement, which is inconveniently placed within the working window of batteries.[203]

Sodium ion migration within these materials is dominated by an interlayer diffusion within the [112] and [121] planes, connecting the Na1 and Na2 sites. Another migration path exists perpendicular to these planes connecting Na1 positions within different layers of sodium, which shows a much higher migration barrier. The ion mobility along the migration pathways of the NASICON structure is dominantly determined by either the formation energy of the TM redox couple or the size of the two distinct bottlenecks along the diffusion path. In the case of the bottleneck size being the determining factor, changing the elements that compose the material or introducing dopants can highly influence the migration properties.[206] Typical measured diffusion coefficients for this material are in the range of 10^{-9} - 10^{-11} cm^2 s^{-1}, with outliers of up to 10^{-8} cm^2 s^{-1} or down to 10^{-15} cm^2 s^{-1}.[203,207] Theoretically calculated values for migration barriers agree well with experimentally reported data, showing migration barriers of 0.3 - 0.6 eV.[203,208] Furthermore, a significant lowering of the migration barriers due to a concerted ion movement was observed theoretically.[209]

Due to their higher charge and therefore lower occupation of crystal sites, multivalent ions like magnesium or calcium only occupy the Na1-position within the NASICON framework.

The approach of utilizing multivalent charge carriers could therefore circumvent the issue of a structural change within the working window and the halved occupation of the sodium sites leads to higher structural rigidity. Unfortunately, this also creates a longer diffusion path (no intermediate at Na2) and a more sluggish migration owed to the increased electrostatic interactions with the framework. An extensive overview over the properties of this material class can be found in the report of Alamo.[210]

5.9 Anion migrations

Whilst cation migration is well studied, less work has been done regarding the migration of anions in crystalline structures which may be used as solid state electrolytes (SSE) in the growing field of halide (fluoride or chloride) ion batteries.[211–214] The most studied materials usable as SSEs in fluoride ion batteries (FIBs) are based on either rare-earth tysonite-type structures RF_3 (R=La, Ce, Sm) or alkaline-earth fluorite-type structures MF_2 (M=Ca, Ba, Sr). Ionic conductivity in tysonite-type fluorides happens by a vacancy mechanism via intrinsic Schottky defects, whereas it occurs in the fluorite-structures due to an anionic interstitial mechanism via intrinsic anti-Frenkel pairs. By homogeneous doping, the ionic conductivity can be significantly increased, as aliovalent cation substitution creates extrinsic defects, i.e., anionic vacancies, in case of doped tysonite-type solid solutions $R_{1-x}M_xF_{3-x}$, or interstitials, in case of doped fluorite-type solid solutions $M_{1-x}R_xF_{2+x}$.[215] The first rechargeable FIB employed the nanocrystalline Ba-doped tysonite $La_{0.9}Ba_{0.1}F_{2.9}$ as SSE with an fluoride ion conductivity of 2.8×10^{-4} S cm^{-1} at 160°C.[216] By employing single crystals of $La_{0.9}Ba_{0.1}F_{2.9}$, a comparable ion conductivity can already be achieved at room temperature. Yet, as single crystals are difficult to implement into batteries, attempts to improve the ionic conductivity of polycrystalline materials have been made. In detailed studies on the ion conduction mechanism in FIBs, Rongeat et al. revealed, that grain boundaries lead to noticeable blocking effects in tysonite-type fluorides and that heat treatment of the polycrystalline tysonite-type SSE can significantly enhance the ionic conductivity.[217] In contrast, due to the different

ion conduction mechanism in fluorite-type materials, the ionic conductivity of the La-doped fluorite $Ba_{1-x}La_xF_{2+x}$ can be improved by increasing the number of grain boundaries via nanostructuring, as it offers additional conduction paths for the motion of vacancies along the grain boundaries, yielding an optimum ionic conductivity for $Ba_{0.6}La_{0.4}F_{2.4}$ of 1.9×10^{-4}S cm^{-1} at 160°C.[218] Yet, for the polycrystalline fluorite- or tysonite-type compounds discussed so far sufficient ion conductivity can only be achieved at temperatures above 150°C. Only in form of sintered disks, which cannot be integrated into batteries, $Sm_{0.95}Ca_{0.05}F_{2.95}$ and $Ce_{0.975}Sr_{0.025}F_{2.975}$ yield conductivities of 1×10^{-4} S cm^{-1} or 3×10^{-4} S cm^{-1} at room temperature.[219,220] Still, Dieudonné et al. employed these systematic studies with Ca- and Sr-doped tysonite-type SmF_3 or CeF_3 structures[219,220] to reveal valuable structure-property-relations: they found that the difference between the ionic radii of M^{2+} and R^{3+} plays a key role for structural features such as buckling effects which in turn have a strong impact on the fluoride conductivity. As outlined earlier, such a relationship can assist the search for new ionic conductors.

Besides, ternary systems, such as the Sn-based metal fluorides $MSnF_4$ (M=Pb, Ba, Sr), show a very high ionic conductivity (10^{-3} to 10^{-4} S cm^{-1}) at room temperature.[221] The superionic conductivity has been related to the disorder caused by the stereo-activity of Sn^{2+} lone pairs.[222] Repulsive interactions between the electron lone pair and F ions occur, leading to a depletion of F ions in the Sn^{2+} containing layers of the crystal and an increase in the fluoride ion mobility within these layers.[213] Mohammad et al. proved that $BaSnF_4$ can be used as solid electrolyte in room temperature FIBs.[223]

Finally, the corner-sharing network of the octahedral building blocks in halide perovskites ABX_3 can also allow facile, vacancy-mediated anion migration.[224] By employing a K-doped $CsPbF_3$ perovskite ($CsPb_{0.9}K_{0.1}F_{2.9}$) an ionic conductivity of 1.23×10^{-3} S cm^{-1} at room temperature could be achieved by Wang et al.[225] Moreover, this fluoride conducting SSE exhibits an electrochemical stability window (ESW), which is significantly wider than that of $BaSnF_4$ or $PbSnF_4$.[225] Such a desired combination of a high ion conductivity at room tem-

perature and a high electrochemical stability has also been found for the chloride perovskite $CsSnCl_3$ (σ=3.6×10^{-4} S cm^{-1}, width of ESW: 6.1 V) which can be used as SSE for chloride ion batteries. In this study the creation of a high amount of nanograins, lattice strain and tin vacancies during synthesis assured the structural stability of the cubic $CsSnCl_3$ phase against transition to its monoclinic phase.[226]

Trends in the migration barriers within different halide perovskites have been explained by the trends in the B-X covalency: the stronger the covalent character the higher the ion migration barrier.[224,227] Covalency has been determined either by the relative energetic positions of the band center of the B-site cation and the isolated halogen atom[224] or based on the crystal orbital Hamiltonian population.[227] These or similar descriptors might be useful for the development of further SSEs in halide ion batteries.

6 Conclusion and perspective

This review emphasizes the ion mobility in crystalline battery materials, encompassing both electrolytes and electrodes, and reveals a crucial distinction between their roles. Electrolytes act as ion conductors while maintaining the role of an electronic insulators to prevent the uncontrolled flow of electrons during battery operation. On the other hand, electrodes must serve as both ion and electron conductors to facilitate the recombination of ions and electrons upon their entry into the electrodes. Despite these divergent functions, from a quantum chemical perspective, the determination of migration properties depends on the minimum energy path connecting two equivalent intercalation sites and the maximum activation barrier along this path. This insight highlights the essential similarity in the migration behavior of ions in both electrolytes and electrodes, emphasizing the importance of understanding and optimizing ion mobility for the development of advanced and efficient battery materials.

We explored the potential for establishing descriptors for ionic conductivities that can universally correlate across different structural families. Such descriptors could greatly ac-

celerate the discovery of new ion conductors with superionic conductivity. High ionic conductivity has been correlated with electrodes and electrolytes featuring body-centered cubic anion sublattices and structures where the mobile species is not in its preferred coordination. Besides this structural considerations, the connection between ionic size, oxidation state, and electronegativity of compound species can describe ionic conductivity for various cation and anion chemistries in different structural families. Furthermore, within the spinel structure, the migration barrier of mobile cations demonstrates a volcano-like trend, where the optimal activation energies are achieved when the site preference between two inequivalent minima tends towards zero. These correlations suggest a promising path for identifying new superionic conductors. Moreover, enhancing ionic conductivities among different types of materials including silver, sodium, lithium, and fluorine ions, has been demonstrated by lowering the frequency of low-energy optical phonons. These hypotheses, however require further experimental and computational investigation.

Little attention has been paid so far to limitations of the ion mobility due to structural constraints at the interface between the solid electrolyte and electrode. The interaction between solid-state electrolytes and electrode materials can limit the practical use in batteries as it may lead to interfacial structures that impede the transfer of ions. The reasons for these behavior are not well understood yet. Future research is necessary to comprehend the reaction mechanisms at the interface between fast ion conductors and conventional electrode materials, as well as between different fast ion conductors. The goal is to develop solutions that stabilize these interfaces. Understanding and controlling interfacial reactivity is crucial for leveraging space charge layers created in multicomponent ion conductors for enhanced ion conductivity through nanostructural designs. It is also important to minimize interface reactivity by protecting ion conductors with surface coatings.

References

(1) Bachman, J. C.; Muy, S.; Grimaud, A.; Chang, H.-H.; Pour, N.; Lux, S. F.; Paschos, O.; Maglia, F.; Lupart, S.; Lamp, P.; Giordano, L.; Shao-Horn, Y. Inorganic Solid-State Electrolytes for Lithium Batteries: Mechanisms and Properties Governing Ion Conduction. *Chem. Rev.* **2016**, *116*, 140–162.

(2) Sotoudeh, M.; Dillenz, M.; Groß, A. Mechanism of Magnesium Transport in Spinel Chalcogenides. *Adv. Energy Sustainability Res.* **2021**, *2*, 2100113.

(3) Sotoudeh, M.; Groß, A. Descriptor and Scaling Relations for Ion Mobility in Crystalline Solids. *JACS Au* **2022**, *2*, 463–471.

(4) Dillenz, M.; Sotoudeh, M.; Glaser, C.; Janek, J.; Groß, A.; Euchner, H. Unravelling Charge Carrier Mobility in d_0-Metal-based Spinels. *Batter. Supercaps* **2022**, *5*, e202200164.

(5) Helmbrecht, K.; Euchner, H.; Groß, A. Revisiting the Chevrel Phase: Impact of Dispersion Corrections on the Properties of Mo_6S_8 for Cathode Applications. *Batter. Supercaps* **2022**, *5*, e202200002.

(6) Famprikis, T.; Canepa, P.; Dawson, J. A.; Islam, M. S.; Masquelier, C. Fundamentals of inorganic solid-state electrolytes for batteries. *Nat. Mater.* **2019**, *18*, 1278–1291.

(7) Wert, C. A. Diffusion Coefficient of C in α-Iron. *Phys. Rev.* **1950**, *79*, 601–605.

(8) Vineyard, G. H. Frequency factors and isotope effects in solid state rate processes. *J. Phys. Chem. Sol.* **1957**, *3*, 121–127.

(9) Hänggi, P.; Talkner, P.; Borkovec, M. Reaction-rate theory: fifty years after Kramers. *Rev. Mod. Phys.* **1990**, *62*, 251.

(10) Frenkel, J. Über die Wärmebewegung in festen und flüssigen Körpern. *Z. Physik* **1926**, *35*, 652–669.

(11) Wagner, C.; Schottky, W. Theorie der geordneten Mischphasen. *Z. Phys. Chem. B* **1930**, *11*, 163–210.

(12) Mehrer, H. *Diffusion in Solids: Fundamentals, Methods, Materials, Diffusion-Controlled Processes*; Springer Series in Solid-State Sciences; Springer Berlin Heidelberg, 2007.

(13) Mahlberg, D.; Groß, A. Vacancy assisted diffusion on single-atom surface alloys. *ChemPhysChem* **2021**, *22*, 29–39.

(14) Tubandt, C.; Lorenz, E. Molekularzustand und elektrisches Leitvermögen kristallisierter Salze. *Z. Phys. Chem.* **1914**, *87U*, 513–542.

(15) Friauf, R. J. Diffusion of Silver in Silver Bromide and Evidence for Interstitialcy Migration. *Phys. Rev.* **1957**, *105*, 843–848.

(16) Friauf, R. J. Correlation Effects for Diffusion in Ionic Crystals. *J. Appl. Phys.* **2004**, *33*, 494–505.

(17) Grinderslev, J. B.; Skov, L. N.; Andreasen, J. G.; Ghorwal, S.; Skibsted, J.; Jensen, T. R. Methylamine Lithium Borohydride as Electrolyte for All-Solid-State Batteries. *Angew. Chem., Int. Ed.* **2022**, *61*, e202203484.

(18) Yan, Y.; Dononelli, W.; Jørgensen, M.; Grinderslev, J. B.; Lee, Y.-S.; Cho, Y. W.; Černỳ, R.; Hammer, B.; Jensen, T. R. The mechanism of Mg^{2+} conduction in ammine magnesium borohydride promoted by a neutral molecule. *Phys. Chem. Chem. Phys.* **2020**, *22*, 9204–9209.

(19) Janek, J.; Zeier, W. G. Challenges in speeding up solid-state battery development. *Nat. Energy* **2023**, *8*, 230–240.

(20) Chen, T.; Ceder, G.; Sai Gautam, G.; Canepa, P. Evaluation of Mg Compounds as Coating Materials in Mg Batteries. *Front. Chem.* **2019**, *7*, 24.

(21) Chen, T.; Sai Gautam, G.; Canepa, P. Ionic Transport in Potential Coating Materials for Mg Batteries. *Chem. Mater.* **2019**, *31*, 8087–8099.

(22) Sotoudeh, M.; Groß, A. Stability of Magnesium Binary and Ternary Compounds for Batteries Determined from First Principles. *J. Phys. Chem. Lett.* **2022**, *13*, 10092–10100.

(23) Ikeda, S.; Takahashi, M.; Ishikawa, J.; Ito, K. Solid electrolytes with multivalent cation conduction. 1. Conducting species in Mg-Zr-PO_4 system. *Solid State Ion.* **1987**, *23*, 125 – 129.

(24) Halim, Z.; Adnan, S.; Mohamed, N. Effect of sintering temperature on the structural, electrical and electrochemical properties of novel $Mg_{0.5}Si_2(PO_4)_3$ ceramic electrolytes. *Ceram. Int.* **2016**, *42*, 4452 – 4461.

(25) Mohtadi, R.; Matsui, M.; Arthur, T. S.; Hwang, S.-J. Magnesium Borohydride: From Hydrogen Storage to Magnesium Battery. *Angew. Chem. Int. Ed.* **2012**, *51*, 9780–9783.

(26) Unemoto, A.; Matsuo, M.; Orimo, S.-i. Complex Hydrides for Electrochemical Energy Storage. *Adv. Funct. Mater.* **2014**, *24*, 2267–2279.

(27) Higashi, S.; Miwa, K.; Aoki, M.; Takechi, K. A novel inorganic solid state ion conductor for rechargeable Mg batteries. *Chem. Commun.* **2014**, *50*, 1320–1322.

(28) Canepa, P.; Bo, S.-H.; Sai Gautam, G.; Key, B.; Richards, W. D.; Shi, T.; Tian, Y.; Wang, Y.; Li, J.; Ceder, G. High magnesium mobility in ternary spinel chalcogenides. *Nat. Commun.* **2017**, *8*, 1759.

(29) Koettgen, J.; Bartel, C. J.; Ceder, G. Computational investigation of chalcogenide spinel conductors for all-solid-state Mg batteries. *Chem. Commun.* **2020**, *56*, 1952–1955.

(30) Dillenz, M.; Sotoudeh, M.; Euchner, H.; Groß, A. Screening of Charge Carrier Migration in the $MgSc_2Se_4$ Spinel Structure. *Front. Energy Res.* **2020**, *8*, 260.

(31) Liu, M.; Rong, Z.; Malik, R.; Canepa, P.; Jain, A.; Ceder, G.; Persson, K. A. Spinel compounds as multivalent battery cathodes: a systematic evaluation based on ab initio calculations. *Energy Environ. Sci.* **2015**, *8*, 964–974.

(32) Frank, F. C.; Turnbull, D. Mechanism of Diffusion of Copper in Germanium. *Phys. Rev.* **1956**, *104*, 617–618.

(33) Gösele, U.; Frank, W.; Seeger, A. Mechanism and kinetics of the diffusion of gold in silicon. *Appl. Phys.* **1980**, *23*, 361–368.

(34) Tan, T. Y.; Gösele, U. In *Diffusion in Condensed Matter: Methods, Materials, Models*; Heitjans, P., Kärger, J., Eds.; Springer Berlin Heidelberg: Berlin, Heidelberg, 2005; pp 165–208.

(35) Sakong, S.; Mosch, C.; Lozano, A.; Busnengo, H. F.; Groß, A. Lowering Energy Barriers in Surface Reactions through Concerted Reaction Mechanisms. *ChemPhysChem* **2012**, *13*, 3467–3471.

(36) Thangadurai, V.; Kaack, H.; Weppner, W. J. F. Novel Fast Lithium Ion Conduction in Garnet-Type $Li_5La_3M_2O_{12}$ (M = Nb, Ta). *J. Am. Ceram. Soc.* **2003**, *86*, 437–440.

(37) Allen, J.; Wolfenstine, J.; Rangasamy, E.; Sakamoto, J. Effect of substitution (Ta, Al, Ga) on the conductivity of $Li_7La_3Zr_2O_{12}$. *J. Power Sources* **2012**, *206*, 315–319.

(38) He, X.; Zhu, Y.; Mo, Y. Origin of fast ion diffusion in super-ionic conductors. *Nat. Commun.* **2017**, *8*, 15893.

(39) Doliwa, B.; Heuer, A. Cooperativity and spatial correlations near the glass transition: Computer simulation results for hard spheres and disks. *Phys. Rev. E* **2000**, *61*, 6898.

(40) Marcolongo, A.; Marzari, N. Ionic correlations and failure of Nernst-Einstein relation in solid-state electrolytes. *Phys. Rev. Mater.* **2017**, *1*, 025402.

(41) Kozinsky, B. In *Handbook of Materials Modeling: Applications: Current and Emerging Materials*; Andreoni, W., Yip, S., Eds.; Springer International Publishing: Cham, 2018; pp 1–20.

(42) He, X.; Zhu, Y.; Mo, Y. Origin of fast ion diffusion in super-ionic conductors. *Nat. Commun.* **2017**, *8*, 15893.

(43) Jalem, R.; Yamamoto, Y.; Shiiba, H.; Nakayama, M.; Munakata, H.; Kasuga, T.; Kanamura, K. Concerted migration mechanism in the Li ion dynamics of garnet-type Li7La3Zr2O12. *Chem. Mater.* **2013**, *25*, 425–430.

(44) Zhou, L.; Minafra, N.; Zeier, W. G.; Nazar, L. F. Innovative approaches to Li-argyrodite solid electrolytes for all-solid-state lithium batteries. *Acc. Chem. Res.* **2021**, *54*, 2717–2728.

(45) Richards, W. D.; Tsujimura, T.; Miara, L. J.; Wang, Y.; Kim, J. C.; Ong, S. P.; Uechi, I.; Suzuki, N.; Ceder, G. Design and synthesis of the superionic conductor $Na_{10}SnP_2S_{12}$. *Nat. Commun.* **2016**, *7*, 11009.

(46) Zhou, L.; Assoud, A.; Zhang, Q.; Wu, X.; Nazar, L. F. New family of argyrodite thioantimonate lithium superionic conductors. *J. Am. Chem. Soc.* **2019**, *141*, 19002–19013.

(47) Chen, Y.; Bartel, C. J.; Avdeev, M.; Zhang, Y.-Q.; Liu, J.; Zhong, P.; Zeng, G.; Cai, Z.; Kim, H.; Ji, H., et al. Solid-State Calcium-Ion Diffusion in $Ca_{1.5}Ba_{0.5}Si_5O_3N_6$. *Chem. Mater.* **2021**, *34*, 128–139.

(48) Frenking, G.; Krapp, A. Unicorns in the world of chemical bonding models. *J. Comput. Chem.* **2007**, *28*, 15–24.

(49) Cho, M.; Sylvetsky, N.; Eshafi, S.; Santra, G.; Efremenko, I.; Martin, J. M. L. The Atomic Partial Charges Arboretum: Trying to See the Forest for the Trees. *ChemPhysChem* **2020**, *21*, 688–696.

(50) Zhao, J.; Zhu, Z.-W.; Zhao, D.-X.; Yang, Z.-Z. Atomic charges in molecules defined by molecular real space partition into atomic subspaces. *Phys. Chem. Chem. Phys.* **2023**, *25*, 9020–9030.

(51) Eugen Schwarz, W. H. Richard F. Bader: Atoms in Molecules (A Quantum Theory) Clarendon Press 1990, Oxford. ISBN 019-855-1681. *Berichte der Bunsengesellschaft für physikalische Chemie* **1991**, *95*, 1308–1308.

(52) Béjar, J.; Álvarez–Contreras, L.; Espinosa–Magaña, F.; Ledesma–García, J.; Arjona, N.; Arriaga, L. G. Zn–air battery operated with a 3DOM trimetallic spinel ($Mn_{0.5}Ni_{0.5}Co_2O_4$) as the oxygen electrode. *Electrochim. Acta* **2021**, *391*, 138900.

(53) Kwon, B. J. et al. High Voltage Mg-Ion Battery Cathode via a Solid Solution Cr–Mn Spinel Oxide. *Chem. Mater.* **2020**, *32*, 6577–6587.

(54) Li, L.; Gan, Y.-M.; Lu, Z.-H.; XiaohuYu,; Qing, S.; Gao, Z.; Zhang, R.; Feng, G. The effects of Fe, Co and Ni doping in $CuAl_2O_4$ spinel surface and bulk: A DFT study. *Appl. Surf. Sci.* **2020**, *521*, 146478.

(55) Zasada, F.; Pinho, P. V. B.; Piskorz, W.; Hudy, C.; Janas, J.; Gryboś, J.; Góra-Marek, K.; Sojka, Z. Adsorption of NO_2 and NO_3 on Cobalt Spinel Nanocubes and Interfacial Dynamics of the Resultant NO_x Adspecies (x = 1, 2, and 3): DFT, Atomistic Thermodynamic, IR, and Isotopic Exchange Study. *J. Phys. Chem. C* **2020**, *124*, 19681–19697.

(56) Cao, Y.; Liang, J.; Li, X.; Yue, L.; Liu, Q.; Lu, S.; Asiri, A. M.; Hu, J.; Luo, Y.; Sun, X. Recent advances in perovskite oxides as electrode materials for supercapacitors. *Chem. Commun.* **2021**, *57*, 2343–2355.

(57) Zhao, C.; Yao, Z.; Wang, Q.; Li, H.; Wang, J.; Liu, M.; Ganapathy, S.; Lu, Y.; Cabana, J.; Li, B.; Bai, X.; Aspuru-Guzik, A.; Wagemaker, M.; Chen, L.; Hu, Y.-S. Revealing High Na-Content P2-Type Layered Oxides as Advanced Sodium-Ion Cathodes. *J. Am. Chem. Soc.* **2020**, *142*, 5742–5750.

(58) Pramanik, A.; Manche, A. G.; Clulow, R.; Lightfoot, P.; Armstrong, A. R. Exploiting anion and cation redox chemistry in lithium-rich perovskite oxalate: a novel next-generation Li/Na-ion battery electrode. *Dalton Trans.* **2022**, *51*, 12467–12475.

(59) He, X.; Sun, H.; Ding, X.; Zhao, K. Grain Boundaries and Their Impact on Li Kinetics in Layered-Oxide Cathodes for Li-Ion Batteries. *J. Phys. Chem. C* **2021**, *125*, 10284–10294.

(60) Mulliken, R. S. Electronic Population Analysis on LCAO–MO Molecular Wave Functions. I. *J. Chem. Phys.* **2004**, *23*, 1833–1840.

(61) Hammouri, M.; Arsentev, M.; Petrov, A. Ab initio studies of Ti_2S_3 as a new cathode material for magnesium secondary batteries. *Mater. Today. Commun.* **2019**, *20*, 100598.

(62) Yu, F.-D.; Que, L.-F.; Xu, C.-Y.; Wang, M.-J.; Sun, G.; Duh, J.-G.; Wang, Z.-B. Dual conductive surface engineering of Li-Rich oxides cathode for superior high-energy-density Li-Ion batteries. *Nano Energy* **2019**, *59*, 527–536.

(63) Heidar-Zadeh, F.; Ayers, P. W.; Verstraelen, T.; Vinogradov, I.; Vöhringer-Martinez, E.; Bultinck, P. Information-Theoretic Approaches to Atoms-in-Molecules: Hirshfeld Family of Partitioning Schemes. *J. Phys. Chem. A* **2018**, *122*, 4219–4245.

(64) Xu, Z.; Chen, X.; Liu, K.; Chen, R.; Zeng, X.; Zhu, H. Influence of Anion Charge on Li Ion Diffusion in a New Solid-State Electrolyte, Li_3LaI_6. *Chem. Mater.* **2019**, *31*, 7425–7433.

(65) Fonseca Guerra, C.; Handgraaf, J.-W.; Baerends, E. J.; Bickelhaupt, F. M. Voronoi deformation density (VDD) charges: Assessment of the Mulliken, Bader, Hirshfeld, Weinhold, and VDD methods for charge analysis. *J. Comp. Chem.* **2004**, *25*, 189–210.

(66) Sozykin, S. A.; Beskachko, V. P. Li-decorated carbon nanotubes: charge analysis. *Fuller. Nanotub.* **2022**, *30*, 199–204.

(67) Ullah, S.; Denis, P. A.; Sato, F. Monolayer boron-arsenide as a perfect anode for alkali-based batteries with large storage capacities and fast mobilities. *Int. J. Quantum Chem.* **2019**, *119*, e25975.

(68) Wang, B.; Li, S. L.; Truhlar, D. G. Modeling the Partial Atomic Charges in Inorganometallic Molecules and Solids and Charge Redistribution in Lithium-Ion Cathodes. *J. Chem. Theory Comput.* **2014**, *10*, 5640–5650.

(69) Han, B.; Isborn, C. M.; Shi, L. Determining Partial Atomic Charges for Liquid Water: Assessing Electronic Structure and Charge Models. *J. Chem. Theory Comput.* **2021**, *17*, 889–901.

(70) Ertural, C.; Stoffel, R. P.; Müller, P. C.; Vogt, C. A.; Dronskowski, R. First-Principles Plane-Wave-Based Exploration of Cathode and Anode Materials for Li- and Na-Ion Batteries Involving Complex Nitrogen-Based Anions. *Chem. Mater.* **2022**, *34*, 652–668.

(71) Posysaev, S.; Miroshnichenko, O.; Alatalo, M.; Le, D.; Rahman, T. S. Oxidation states of binary oxides from data analytics of the electronic structure. *Comput. Mater. Sci.* **2019**, *161*, 403–414.

(72) Ghiringhelli, L. M.; Vybiral, J.; Levchenko, S. V.; Draxl, C.; Scheffler, M. Big Data of Materials Science: Critical Role of the Descriptor. *Phys. Rev. Lett.* **2015**, *114*, 105503.

(73) Isayev, O.; Oses, C.; Toher, C.; Gossett, E.; Curtarolo, S.; Tropsha, A. Universal fragment descriptors for predicting properties of inorganic crystals. *Nat. Commun.* **2017**, *8*, 15679.

(74) Nørskov, J. K.; Rossmeisl, J.; Logadottir, A.; Lindqvist, L.; Kitchin, J. R.; Bligaard, T.; Jónsson, H. Origin of the Overpotential for Oxygen Reduction at a Fuel-Cell Cathode. *J. Phys. Chem. B* **2004**, *108*, 17886–17892.

(75) Man, I. C.; Su, H.-Y.; Calle-Vallejo, F.; Hansen, H. A.; Martinez, J. I.; Inoglu, N. G.; Kitchin, J.; Jaramillo, T. F.; Nørskov, J. K.; Rossmeisl, J. Universality in Oxygen Evolution Electrocatalysis on Oxide Surfaces. *ChemCatChem* **2011**, *3*, 1159–1165.

(76) Jäckle, M.; Helmbrecht, K.; Smits, M.; Stottmeister, D.; Groß, A. Self-diffusion barriers: Possible descriptors for dendrite growth in batteries? *Energy Environ. Sci.* **2018**, *11*, 3400–3407.

(77) Wang, Y.; Richards, W. D.; Ong, S. P.; Miara, L. J.; Kim, J. C.; Mo, Y.; Ceder, G. Design principles for solid-state lithium superionic conductors. *Nat. Mater.* **2015**, *14*, 1026.

(78) Muy, S.; Bachman, J. C.; Giordano, L.; Chang, H.-H.; Abernathy, D. L.; Bansal, D.; Delaire, O.; Hori, S.; Kanno, R.; Maglia, F.; Lupart, S.; Lamp, P.; Shao-Horn, Y. Tuning mobility and stability of lithium ion conductors based on lattice dynamics. *Energy Environ. Sci.* **2018**, *11*, 850–859.

(79) Gordiz, K.; Muy, S.; Zeier, W. G.; Shao-Horn, Y.; Henry, A. Enhancement of ion diffusion by targeted phonon excitation. *Cell Rep.* **2021**, *2*, 100431.

(80) Rong, Z.; Malik, R.; Canepa, P.; Sai Gautam, G.; Liu, M.; Jain, A.; Persson, K.; Ceder, G. Materials Design Rules for Multivalent Ion Mobility in Intercalation Structures. *Chem. Mater.* **2015**, *27*, 6016–6021.

(81) Sotoudeh, M.; Dillenz, M.; Döhn, J.; Hansen, J.; Dsoke, S.; Groß, A. Oxide Spinels with Superior Mg Conductivity. *Chem. Mater.* **2023**, *35*, 4786–4797.

(82) Kim, K.; Siegel, D. J. Machine learning reveals factors that control ion mobility in anti-perovskite solid electrolytes. *J. Mater. Chem. A* **2022**, *10*, 15169–15182.

(83) Jalem, R.; Nakayama, M.; Kasuga, T. An efficient rule-based screening approach for discovering fast lithium ion conductors using density functional theory and artificial neural networks. *J. Mater. Chem. A* **2014**, *2*, 720–734.

(84) Jalem, R.; Kimura, M.; Nakayama, M.; Kasuga, T. Informatics-Aided Density Functional Theory Study on the Li Ion Transport of Tavorite-Type $LiMTO_4F$ (M^{3+}–T^{5+}, M^{2+}–T^{6+}). *J. Chem. Inf. Model.* **2015**, *55*, 1158–1168.

(85) Kireeva, N.; Pervov, V. S. Materials space of solid-state electrolytes: unraveling chemical composition–structure–ionic conductivity relationships in garnet-type metal oxides using cheminformatics virtual screening approaches. *Phys. Chem. Chem. Phys.* **2017**, *19*, 20904–20918.

(86) Sendek, A. D.; Yang, Q.; Cubuk, E. D.; Duerloo, K.-A. N.; Cui, Y.; Reed, E. J. Holistic computational structure screening of more than 12000 candidates for solid lithium-ion conductor materials. *Energy Environ. Sci.* **2017**, *10*, 306–320.

(87) Ling, C.; Mizuno, F. Phase stability of post-spinel compound AMn_2O_4 (A= Li, Na, or Mg) and its application as a rechargeable battery cathode. *Chem. Mater.* **2013**, *25*, 3062–3071.

(88) Euchner, H.; Clemens, O.; Reddy, M. A. Unlocking the potential of weberite-type metal fluorides in electrochemical energy storage. *Npj Comput. Mater.* **2019**, *5*, 31.

(89) Rutt, A.; Sari, D.; Chen, Q.; Kim, J.; Ceder, G.; Persson, K. A. Novel Structural Motif

To Promote Mg-Ion Mobility: Investigating ABO_4 Zircons as Magnesium Intercalation Cathodes. *ACS Appl. Mater. Interfaces* **2023**,

(90) Yang, S.-H.; Xue, H.; Guo, S.-P. Borates as promising electrode materials for rechargeable batteries. *Coord. Chem. Rev.* **2021**, *427*, 213551.

(91) Zhang, N.; Dong, Y.; Jia, M.; Bian, X.; Wang, Y.; Qiu, M.; Xu, J.; Liu, Y.; Jiao, L.; Cheng, F. Rechargeable aqueous Zn–V_2O_5 battery with high energy density and long cycle life. *ACS Energy Lett.* **2018**, *3*, 1366–1372.

(92) Campanella, L.; Pistoia, G. MoO_3: a new electrode material for nonaqueous secondary battery applications. *J. Electrochem. Soc.* **1971**, *118*, 1905.

(93) Lahan, H.; Das, S. K. Al^{3+} ion intercalation in MoO_3 for aqueous aluminum-ion battery. *J. Power Sources* **2019**, *413*, 134–138.

(94) Bayliss, R. D.; Key, B.; Sai Gautam, G.; Canepa, P.; Kwon, B. J.; Lapidus, S. H.; Dogan, F.; Adil, A. A.; Lipton, A. S.; Baker, P. J.; Ceder, G.; Vaughey, J. T.; Cabana, J. Probing Mg Migration in Spinel Oxides. *Chem. Mater.* **2020**, *32*, 663–670.

(95) Chen, T.; Sai Gautam, G.; Huang, W.; Ceder, G. First-Principles Study of the Voltage Profile and Mobility of Mg Intercalation in a Chromium Oxide Spinel. *Chem. Mater.* **2018**, *30*, 153–162.

(96) Padhi, A. K.; Nanjundaswamy, K. S.; Goodenough, J. B. Phospho-olivines as positive-electrode materials for rechargeable lithium batteries. *J. Electrochem. Soc.* **1997**, *144*, 1188.

(97) Wang, Y.; Chen, R.; Chen, T.; Lv, H.; Zhu, G.; Ma, L.; Wang, C.; Jin, Z.; Liu, J. Emerging non-lithium ion batteries. *Energy Storage Mater.* **2016**, *4*, 103–129.

(98) Lee, K. T.; Ramesh, T.; Nan, F.; Botton, G.; Nazar, L. F. Topochemical synthesis

of sodium metal phosphate olivines for sodium-ion batteries. *Chem. Mater.* **2011**, *23*, 3593–3600.

(99) Alfaruqi, M. H.; Kim, S.; Park, S.; Lee, S.; Lee, J.; Hwang, J.-Y.; Sun, Y.-K.; Kim, J. Density functional theory investigation of mixed transition metals in olivine and tavorite cathode materials for Li-ion batteries. *ACS Appl. Mater. Interfaces* **2020**, *12*, 16376–16386.

(100) Tolganbek, N.; Yerkinbekova, Y.; Kalybekkyzy, S.; Bakenov, Z.; Mentbayeva, A. Current state of high voltage olivine structured $LiMPO_4$ cathode materials for energy storage applications: A review. *J. Alloys Compd.* **2021**, *882*, 160774.

(101) Amin, R.; Maier, J.; Balaya, P.; Chen, D.; Lin, C. Ionic and electronic transport in single crystalline $LiFePO_4$ grown by optical floating zone technique. *Solid State Ion.* **2008**, *179*, 1683–1687.

(102) Morgan, D.; Van der Ven, A.; Ceder, G. Li conductivity in Li_xMPO_4 (M= Mn, Fe, Co, Ni) olivine materials. *Electrochem. solid-state Lett.* **2003**, *7*, A30.

(103) Adams, S. Lithium ion pathways in $LiFePO_4$ and related olivines. *J. Solid State Electrochem.* **2010**, *14*, 1787–1792.

(104) Malik, R.; Burch, D.; Bazant, M.; Ceder, G. Particle size dependence of the ionic diffusivity. *Nano Lett.* **2010**, *10*, 4123–4127.

(105) Yang, J.; Tse, J. S. Li ion diffusion mechanisms in $LiFePO_4$: an ab initio molecular dynamics study. *J. Phys. Chem. A* **2011**, *115*, 13045–13049.

(106) Delacourt, C.; Laffont, L.; Bouchet, R.; Wurm, C.; Leriche, J.-B.; Morcrette, M.; Tarascon, J.-M.; Masquelier, C. Toward understanding of electrical limitations (electronic, ionic) in $LiMPO_4$ (M= Fe, Mn) electrode materials. *J. Electrochem. Soc.* **2005**, *152*, A913.

(107) Yang, H.; Fu, C.; Sun, Y.; Wang, L.; Liu, T. Fe-doped $LiMnPO_4$@C nanofibers with high Li-ion diffusion coefficient. *Carbon* **2020**, *158*, 102–109.

(108) Kanungo, S.; Bhattacharjee, A.; Bahadursha, N.; Ghosh, A. Comparative Analysis of $LiMPO_4$ (M= Fe, Co, Cr, Mn, V) as Cathode Materials for Lithium-Ion Battery Applications—A First-Principle-Based Theoretical Approach. *Nanomaterials* **2022**, *12*, 3266.

(109) Flack, T.; Jobbins, S. A.; Boulfelfel, S. E.; Leoni, S. Many-Particle Li Ion Dynamics in $LiMPO_4$ Olivine Phosphates (M= Mn, Fe). *J. Phys. Chem. C* **2022**, *126*, 12339–12347.

(110) Anseán, D.; Dubarry, M.; Devie, A.; Liaw, B.; García, V.; Viera, J.; González, M. Operando lithium plating quantification and early detection of a commercial $LiFePO_4$ cell cycled under dynamic driving schedule. *J. Power Sources* **2017**, *356*, 36–46.

(111) Mauger, A.; Julien, C. M. Olivine positive electrodes for Li-ion batteries: Status and perspectives. *Batteries* **2018**, *4*, 39.

(112) Yang, L.; Deng, W.; Xu, W.; Tian, Y.; Wang, A.; Wang, B.; Zou, G.; Hou, H.; Deng, W.; Ji, X. Olivine $LiMn_xFe_{1-x}PO_4$ cathode materials for lithium ion batteries: Restricted factors of rate performances. *J. Mater. Chem. A* **2021**, *9*, 14214–14232.

(113) Thangadurai, V.; Weppner, W. $Li_6ALa_2Nb_2O_{12}$ (A=Ca, Sr, Ba): A New Class of Fast Lithium Ion Conductors with Garnet-Like Structure. *J. Am. Ceram. Soc.* **2005**, *88*, 411–418.

(114) Thangadurai, V.; Weppner, W. Investigations on electrical conductivity and chemical compatibility between fast lithium ion conducting garnet-like $Li_6BaLa_2Ta_2O_{12}$ and lithium battery cathodes. *J. Power Sources* **2005**, *142*, 339–344.

(115) Murugan, R.; Thangadurai, V.; Weppner, W. Lattice Parameter and Sintering Temperature Dependence of Bulk and Grain-Boundary Conduction of Garnet-like Solid Li-Electrolytes. *J. Electrochem. Soc.* **2007**, *155*, A90.

(116) Inaguma, Y.; Liquan, C.; Itoh, M.; Nakamura, T.; Uchida, T.; Ikuta, H.; Wakihara, M. High ionic conductivity in lithium lanthanum titanate. *Solid State Commun.* **1993**, *86*, 689–693.

(117) Belous, A.; Novitskaya, G.; Polyanetskaya, S.; Gornikov, Y. I. Investigation into complex oxides of $La_{2/3-x}Li_{3x}TiO_3$ composition. *Izv. Akad. Nauk SSSR, Neorg. Mater* **1987**, *23*, 470–472.

(118) Stramare, S.; Thangadurai, V.; Weppner, W. Lithium lanthanum titanates: a review. *Chem. Mater.* **2003**, *15*, 3974–3990.

(119) Chen, C.-h.; Du, J. Lithium ion diffusion mechanism in lithium lanthanum titanate solid-state electrolytes from atomistic simulations. *J. Am. Ceram. Soc.* **2015**, *98*, 534–542.

(120) Ibarra, J.; Várez, A.; León, C.; Santamarıa, J.; Torres-Martınez, L.; Sanz, J. Influence of composition on the structure and conductivity of the fast ionic conductors $La_{2/3-x}Li_{3x}TiO_3$ ($0.03 \leq x \leq 0.167$). *Solid State Ion.* **2000**, *134*, 219–228.

(121) Inaguma, Y.; Chen, L.; Itoh, M.; Nakamura, T. Candidate compounds with perovskite structure for high lithium ionic conductivity. *Solid State Ion.* **1994**, *70*, 196–202.

(122) Harada, Y.; Hirakoso, Y.; Kawai, H.; Kuwano, J. Order–disorder of the A-site ions and lithium ion conductivity in the perovskite solid solution $La_{0.67-x}Li_{3x}TiO_3$ (x= 0.11). *Solid State Ion.* **1999**, *121*, 245–251.

(123) Jay, E.; Rushton, M.; Chroneos, A.; Grimes, R.; Kilner, J. Genetics of superionic

conductivity in lithium lanthanum titanates. *Phys. Chem. Chem. Phys.* **2015**, *17*, 178–183.

(124) Symington, A. R.; Purton, J.; Statham, J.; Molinari, M.; Islam, M. S.; Parker, S. C. Quantifying the impact of disorder on Li-ion and Na-ion transport in perovskite titanate solid electrolytes for solid-state batteries. *J. Mater. Chem. A* **2020**, *8*, 19603–19611.

(125) Hasegawa, G.; Kuwata, N.; Hashi, K.; Tanaka, Y.; Takada, K. Lithium-Ion Diffusion in Perovskite-Type Solid Electrolyte Lithium Lanthanum Titanate Revealed by Pulsed-Field Gradient Nuclear Magnetic Resonance. *Chem. Mater.* **2023**, *35*, 3815–3824.

(126) Kobayashi, S.; Yokoe, D.; Fujiwara, Y.; Kawahara, K.; Ikuhara, Y.; Kuwabara, A. Lithium lanthanum titanate single crystals: dependence of lithium-ion conductivity on crystal domain orientation. *Nano Lett.* **2022**, *22*, 5516–5522.

(127) Belous, A.; Pashkova, E.; Gavrilenko, O.; V'yunov, O.; Kovalenko, L. Solid electrolytes based on lithium-containing lanthanum metaniobates. *J. Eur. Ceram. Soc.* **2004**, *24*, 1301–1304.

(128) Yang, Z.; Suzuki, S.; Tanibata, N.; Takeda, H.; Nakayama, M.; Karasuyama, M.; Takeuchi, I. Efficient Experimental Search for Discovering a Fast Li-Ion Conductor from a Perovskite-Type $Li_xLa_{(1-x)/3}NbO_3$ (LLNO) Solid-State Electrolyte Using Bayesian Optimization. *J. Phys. Chem. C* **2020**, *125*, 152–160.

(129) Hong, J.; Kobayashi, S.; Kuwabara, A.; Ikuhara, Y. H.; Fujiwara, Y.; Ikuhara, Y. Defect Engineering and Anisotropic Modulation of Ionic Transport in Perovskite Solid Electrolyte $Li_xLa_{(1-x)/3}NbO_3$. *Molecules* **2021**, *26*, 3559.

(130) Pérez-Vicente, C.; Medina, A.; Alcantara, R. A Comparative View of Alkaline and Alkaline-Earth Element Intercalation into Perovskite-Type $A_xLa_yTiO_3$ (A= Li, Na,

or Mg) Based on Theoretical Calculations and Experiments. *ACS Appl. Energy Mater.* **2022**, *5*, 15749–15757.

(131) Kong, Y.; Liu, Y.; Hu, G. Synthesis and sodium ionic conductivity for perovskite-structured $Na_{0.25}La_{0.25}NbO_3$ ceramic. *Ceram. Int.* **2022**, *48*, 36136–36139.

(132) Zhao, Y.; Liu, Z.; Xu, J.; Zhang, T.; Zhang, F.; Zhang, X. Synthesis and characterization of a new perovskite-type solid-state electrolyte of $Na_{1/3}La_{1/3}Sr_{1/3}ZrO_3$ for all-solid-state sodium-ion batteries. *J. Alloys Compd.* **2019**, *783*, 219–225.

(133) Zhao, Y.; Daemen, L. L. Superionic conductivity in lithium-rich anti-perovskites. *Journal of the American Chemical Society* **2012**, *134*, 15042–15047.

(134) Dawson, J. A.; Famprikis, T.; Johnston, K. E. Anti-perovskites for solid-state batteries: recent developments, current challenges and future prospects. *J. Mater. Chem. A* **2021**, *9*, 18746–18772.

(135) Xia, W.; Zhao, Y.; Zhao, F.; Adair, K.; Zhao, R.; Li, S.; Zou, R.; Zhao, Y.; Sun, X. Antiperovskite electrolytes for solid-state batteries. *Chem. Rev.* **2022**, *122*, 3763–3819.

(136) Sun, Y.; Wang, Y.; Liang, X.; Xia, Y.; Peng, L.; Jia, H.; Li, H.; Bai, L.; Feng, J.; Jiang, H., et al. Rotational cluster anion enabling superionic conductivity in sodium-rich antiperovskite Na_3OBH_4. *J. Am. Chem. Soc.* **2019**, *141*, 5640–5644.

(137) Zhang, Z.; Nazar, L. F. Exploiting the paddle-wheel mechanism for the design of fast ion conductors. *Nat. Rev. Mater.* **2022**, *7*, 389–405.

(138) Keggin, J.; Miles, F. Structures and formulae of the Prussian blues and related compounds. *Nature* **1936**, *137*, 577–578.

(139) Hegner, F. S.; Galán-Mascarós, J. R.; López, N. A database of the structural and electronic properties of Prussian blue, Prussian white, and Berlin green compounds through density functional theory. *Inorg. Chem.* **2016**, *55*, 12851–12862.

(140) Itaya, K.; Uchida, I.; Neff, V. D. Electrochemistry of polynuclear transition metal cyanides: Prussian blue and its analogues. *Acc. Chem. Res.* **1986**, *19*, 162–168.

(141) Itaya, K.; Ataka, T.; Toshima, S. Spectroelectrochemistry and electrochemical preparation method of Prussian blue modified electrodes. *J. Am. Chem. Soc.* **1982**, *104*, 4767–4772.

(142) Kraft, A. Some considerations on the structure, composition, and properties of Prussian blue: a contribution to the current discussion. *Ionics* **2021**, *27*, 2289–2305.

(143) Wang, L.; Song, J.; Qiao, R.; Wray, L. A.; Hossain, M. A.; Chuang, Y.-D.; Yang, W.; Lu, Y.; Evans, D.; Lee, J.-J., et al. Rhombohedral Prussian white as cathode for rechargeable sodium-ion batteries. *J. Am. Chem. Soc.* **2015**, *137*, 2548–2554.

(144) Song, J.; Wang, L.; Lu, Y.; Liu, J.; Guo, B.; Xiao, P.; Lee, J.-J.; Yang, X.-Q.; Henkelman, G.; Goodenough, J. B. Removal of interstitial H_2O in hexacyanometallates for a superior cathode of a sodium-ion battery. *J. Am. Chem. Soc.* **2015**, *137*, 2658–2664.

(145) Wang, W.; Gang, Y.; Hu, Z.; Yan, Z.; Li, W.; Li, Y.; Gu, Q.-F.; Wang, Z.; Chou, S.-L.; Liu, H.-K., et al. Reversible structural evolution of sodium-rich rhombohedral Prussian blue for sodium-ion batteries. *Nat. Commun.* **2020**, *11*, 980.

(146) Herren, F.; Fischer, P.; Ludi, A.; Hälg, W. Neutron diffraction study of Prussian Blue, $Fe_4[Fe(CN)_6]_3.xH_2O$. Location of water molecules and long-range magnetic order. *Inorg. Chem.* **1980**, *19*, 956–959.

(147) Nordstrand, J.; Toledo-Carrillo, E.; Vafakhah, S.; Guo, L.; Yang, H. Y.; Kloo, L.; Dutta, J. Ladder mechanisms of ion transport in Prussian blue analogues. *ACS Appl. Mater. Interfaces* **2021**, *14*, 1102–1113.

(148) Nordstrand, J.; Toledo-Carrillo, E.; Kloo, L.; Dutta, J. Sodium to cesium ions: a

general ladder mechanism of ion diffusion in prussian blue analogs. *Phys. Chem. Chem. Phys.* **2022**, *24*, 12374–12382.

(149) Komayko, A. I.; Arkharova, N. A.; Presnov, D. E.; Levin, E. E.; Nikitina, V. A. Resolving the Seeming Contradiction between the Superior Rate Capability of Prussian Blue Analogues and the Extremely Slow Ionic Diffusion. *J. Phys. Chem.* **2022**, *13*, 3165–3172.

(150) Komayko, A. I.; Ryazantsev, S. V.; Trussov, I. A.; Arkharova, N. A.; Presnov, D. E.; Levin, E. E.; Nikitina, V. A. The Misconception of Mg^{2+} Insertion into Prussian Blue Analogue Structures from Aqueous Solution. *ChemSusChem* **2021**, *14*, 1574–1585.

(151) Shrivastava, A.; Smith, K. C. Electron conduction in nanoparticle agglomerates limits apparent Na^+ diffusion in prussian blue analogue porous electrodes. *J. Electrochem. Soc.* **2018**, *165*, A1777.

(152) Peng, J.; Wang, J.; Yi, H.; Hu, W.; Yu, Y.; Yin, J.; Shen, Y.; Liu, Y.; Luo, J.; Xu, Y., et al. A dual-insertion type sodium-ion full cell based on high-quality ternary-metal Prussian blue analogs. *Adv. Energy Mater.* **2018**, *8*, 1702856.

(153) Baumgart, S.; Sotoudeh, M.; Groß, A. Rhombohedral (R-3) Prussian White as cathode material: An ab-initio study. **2023**, preprint available on ChemXriv at `https://doi.org/10.26434/chemrxiv-2023-qqmqm`.

(154) Ling, C.; Suto, K. Thermodynamic Origin of Irreversible Magnesium Trapping in Chevrel Phase Mo_6S_8: Importance of Magnesium and Vacancy Ordering. *Chem. Mater.* **2017**, *29*, 3731–3739.

(155) Levi, E.; Lancry, E.; Mitelman, A.; Aurbach, D.; Ceder, G.; Morgan, D.; Isnard, O. Phase Diagram of Mg Insertion into Chevrel Phases, $Mg_xMo_6T_8$ (T = S, Se). 1. Crystal Structure of the Sulfides. *Chem. Mater.* **2006**, *18*, 5492–5503.

(156) Kaewmaraya, T.; Ramzan, M.; Osorio-Guillén, J.; Ahuja, R. Electronic structure and ionic diffusion of green battery cathode material: $Mg_2Mo_6S_8$. *Solid State Ion.* **2014**, *261*, 17–20.

(157) Levi, E.; Gershinsky, G.; Aurbach, D.; Isnard, O. Crystallography of Chevrel Phases, MMo_6T_8 (M = Cd, Na, Mn, and Zn, T = S, Se) and Their Cation Mobility. *Inorg. Chem.* **2009**, *48*, 8751–8758.

(158) Thöle, F.; Wan, L. F.; Prendergast, D. Re-examining the Chevrel phase Mo_6S_8 cathode for Mg intercalation from an electronic structure perspective. *Phys. Chem. Chem. Phys.* **2015**, *17*, 22548–22551.

(159) Richard, J.; Benayad, A.; Colin, J.-F.; Martinet, S. Charge Transfer Mechanism into the Chevrel Phase Mo_6S_8 during Mg Intercalation. *J. Phys. Chem. C* **2017**, *121*, 17096–17103.

(160) Aurbach, D.; Lu, Z.; Schechter, A.; Gofer, Y.; Gizbar, H.; Turgeman, R.; Cohen, Y.; Moshkovich, M.; Levi, E. Prototype systems for rechargeable magnesium batteries. *Nature* **2000**, *407*, 724–727.

(161) Mitelman, A.; Levi, M. D.; Lancry, E.; Levi, E.; Aurbach, D. New cathode materials for rechargeable Mg batteries: fast Mg ion transport and reversible copper extrusion in $Cu_yMo_6S_8$ compounds. *Chem. Commun.* **2007**, 4212–4214.

(162) Yoo, H. D.; Shterenberg, I.; Gofer, Y.; Gershinsky, G.; Pour, N.; Aurbach, D. Mg rechargeable batteries: an on-going challenge. *Energy Environ. Sci.* **2013**, *6*, 2265–2279.

(163) Aurbach, D.; Suresh, G.; Levi, E.; Mitelman, A.; Mizrahi, O.; Chusid, O.; Brunelli, M. Progress in Rechargeable Magnesium Battery Technology. *Adv. Mater.* **2007**, *19*, 4260–4267.

(164) Liu, X.; Euchner, H.; Zarrabeitia, M.; Gao, X.; Elia, G. A.; Groß, A.; Passerini, S. Operando pH Measurements Decipher H^+/Zn^{2+} Intercalation Chemistry in High-Performance Aqueous Zn/δ-V_2O_5 Batteries. *ACS Energy Lett.* **2020**, *5*, 2979–2986.

(165) Byeon, P.; Hong, Y.; Bae, H. B.; Shin, J.; Choi, J. W.; Chung, S.-Y. Atomic-scale unveiling of multiphase evolution during hydrated Zn-ion insertion in vanadium oxide. *Nature Comm.* **2021**, *12*, 4599.

(166) Chevrel, R.; Sergent, M.; Prigent, J. Un nouveau sulfure de molybdene : Mo_3S_4 preparation, proprietes et structure cristalline. *Mater. Res. Bull.* **1974**, *9*, 1487–1498.

(167) Canepa, P.; Sai Gautam, G.; Hannah, D. C.; Malik, R.; Liu, M.; Gallagher, K. G.; Persson, K. A.; Ceder, G. Odyssey of Multivalent Cathode Materials: Open Questions and Future Challenges. *Chem. Rev.* **2017**, *117*, 4287–4341.

(168) Juran, T. R.; Smeu, M. Hybrid density functional theory modeling of Ca, Zn, and Al ion batteries using the Chevrel phase Mo_6S_8 cathode. *Phys. Chem. Chem. Phys.* **2017**, *19*, 20684–20690.

(169) Mei, L.; Xu, J.; Wei, Z.; Liu, H.; Li, Y.; Ma, J.; Dou, S. Chevrel Phase Mo_6T_8 (T = S, Se) as Electrodes for Advanced Energy Storage. *Small* **2017**, *13*, 1701441.

(170) Levi, E.; Mitelman, A.; Aurbach, D.; Isnard, O. On the Mechanism of Triclinic Distortion in Chevrel Phase as Probed by In-Situ Neutron Diffraction. *Inorg. Chem.* **2007**, *46*, 7528–7535.

(171) Levi, E.; Mitelman, A.; Isnard, O.; Brunelli, M.; Aurbach, D. Phase Diagram of Mg Insertion into Chevrel Phases, $Mg_xMo_6T_8$ (T = S, Se). 3. The Crystal Structure of Triclinic $Mg_2Mo_6Se_8$. *Inorg. Chem.* **2008**, *47*, 1975–1983.

(172) Smeu, M.; Hossain, S.; Wang, Z.; Timoshevskii, V.; Bevan, K.; Zaghib, K. Theoretical

investigation of Chevrel phase materials for cathodes accommodating Ca^{2+} ions. *J. Power Sources* **2016**, *306*, 431–436.

(173) Rogosic, J. Towards the development of calcium ion batteries. type, PhD Thesis at: Massachusetts Institute of Technology, Department of Materials Science and Engineering,, 2014.

(174) Geng, L.; Lv, G.; Xing, X.; Guo, J. Reversible Electrochemical Intercalation of Aluminum in Mo_6S_8. *Chem. Mater.* **2015**, *27*, 4926–4929.

(175) Lee, B.; Lee, H. R.; Yim, T.; Kim, J. H.; Lee, J. G.; Chung, K. Y.; Cho, B. W.; Oh, S. H. Investigation on the Structural Evolutions during the Insertion of Aluminum Ions into Mo_6S_8 Chevrel Phase. *J. Electrochem. Soc.* **2016**, *163*, A1070.

(176) Cheng, Y.; Luo, L.; Zhong, L.; Chen, J.; Li, B.; Wang, W.; Mao, S. X.; Wang, C.; Sprenkle, V. L.; Li, G.; Liu, J. Highly Reversible Zinc-Ion Intercalation into Chevrel Phase Mo_6S_8 Nanocubes and Applications for Advanced Zinc-Ion Batteries. *ACS Appl. Mater. Interfaces* **2016**, *8*, 13673–13677.

(177) Guohua, L.; Ikuta, H.; Uchida, T.; Wakihara, M. Re-examination of copper Chevrel-phase sulfides as cathode in lithium secondary batteries. *J. Power Sources* **1995**, *54*, 519–521.

(178) Drews, J.; Wiedemann, J.; Maça Alaluf, R. R.; Wang, L.; Blázquez, J. A.; Zhao-Karger, Z.; Fichtner, M.; Danner, T.; Latz, A. Modeling of Magnesium Intercalation into Chevrel Phase Mo_6S_8: Report on Improved Cell Design. *Batter. Supercaps* **2023**, *6*, e202200562.

(179) Li, H.; Okamoto, N. L.; Hatakeyama, T.; Kumagai, Y.; Oba, F.; Ichitsubo, T. Fast Diffusion of Multivalent Ions Facilitated by Concerted Interactions in Dual-Ion Battery Systems. *Adv. Energy Mater.* **2018**, *8*, 1801475.

(180) Delmas, C.; Fouassier, C.; Hagenmuller, P. Structural classification and properties of the layered oxides. *Physica B+C* **1980**, *99*, 81–85.

(181) Van der Ven, A.; Aydinol, M.; Ceder, G.; Kresse, G.; Hafner, J. First-principles investigation of phase stability in Li_xCoO_2. *Phys. Rev. B* **1998**, *58*, 2975.

(182) Reimers, J. N.; Dahn, J. Electrochemical and in situ X-ray diffraction studies of lithium intercalation in Li_xCoO_2. *J. Electrochem. Soc.* **1992**, *139*, 2091.

(183) Delmas, C.; Braconnier, J.-J.; Fouassier, C.; Hagenmuller, P. Electrochemical intercalation of sodium in Na_xCoO_2 bronzes. *Solid State Ion.* **1981**, *3*, 165–169.

(184) Van der Ven, A.; Ceder, G. Lithium diffusion in layered Li_xCoO_2. *Electrochem. Solid-State Lett.* **2000**, *3*, 301.

(185) Van der Ven, A.; Ceder, G.; Asta, M.; Tepesch, P. First-principles theory of ionic diffusion with nondilute carriers. *Phys. Rev. B* **2001**, *64*, 184307.

(186) Mo, Y.; Ong, S. P.; Ceder, G. Insights into diffusion mechanisms in P2 layered oxide materials by first-principles calculations. *Chem. Mater.* **2014**, *26*, 5208–5214.

(187) Ong, S. P.; Chevrier, V. L.; Hautier, G.; Jain, A.; Moore, C.; Kim, S.; Ma, X.; Ceder, G. Voltage, stability and diffusion barrier differences between sodium-ion and lithium-ion intercalation materials. *Energy Environ. Sci.* **2011**, *4*, 3680–3688.

(188) Whittingham, M. S. Electrical energy storage and intercalation chemistry. *Science* **1976**, *192*, 1126–1127.

(189) Whittingham, M. S.; Gamble Jr, F. R. The lithium intercalates of the transition metal dichalcogenides. *Mater. Res. Bull.* **1975**, *10*, 363–371.

(190) Godshall, N. A.; Raistrick, I.; Huggins, R. Thermodynamic investigations of ternary lithium-transition metal-oxygen cathode materials. *Mater. Res. Bull.* **1980**, *15*, 561–570.

(191) Gauckler, C.; Dillenz, M.; Maroni, F.; Pfeiffer, L. F.; Biskupek, J.; Sotoudeh, M.; Fu, Q.; Kaiser, U.; Dsoke, S.; Euchner, H., et al. Detailed Structural and Electrochemical Comparison between High Potential Layered P2-NaMnNi and Doped P2-NaMnNiMg Oxides. *ACS Appl. Energy Mater.* **2022**, *5*, 13735–13750.

(192) Daubner, S.; Dillenz, M.; Pfeiffer, L.; Gauckler, C.; Rosin, M.; Burgard, N.; Martin, J.; Axmann, P.; Sotoudeh, M.; Groß, A.; Schneider, D.; Britta, N. Combined study of phase transitions in the P2-type $Na_xNi_{1/3}Mn_{2/3}O_2$ cathode material: experimental, ab-initio and multiphase-field results. *Research Square* **2023**, https://doi.org/10.21203/rs.3.rs-3125461/v1.

(193) Kim, H.; Seo, D.-H.; Urban, A.; Lee, J.; Kwon, D.-H.; Bo, S.-H.; Shi, T.; Papp, J. K.; McCloskey, B. D.; Ceder, G. Stoichiometric layered potassium transition metal oxide for rechargeable potassium batteries. *Chem. Mater.* **2018**, *30*, 6532–6539.

(194) Tao, Z.-L.; Xu, L.-N.; Gou, X.-L.; Chen, J.; Yuan, H.-T. TiS_2 nanotubes as the cathode materials of Mg-ion batteries. *Chem. Commun.* **2004**, 2080–2081.

(195) Juran, T. R.; Smeu, M. $TiSe_2$ cathode for beyond Li-ion batteries. *J. Power Sources* **2019**, *436*, 226813.

(196) Sun, X.; Bonnick, P.; Nazar, L. F. Layered TiS_2 positive electrode for Mg batteries. *ACS Energy Lett.* **2016**, *1*, 297–301.

(197) Emly, A.; Van der Ven, A. Mg intercalation in layered and spinel host crystal structures for Mg batteries. *Inorg. Chem.* **2015**, *54*, 4394–4402.

(198) Hong, H.-P. Crystal structures and crystal chemistry in the system $Na_{1+x}Zr_2Si_xP_{3-x}O_{12}$. *Mater. Res. Bull.* **1976**, *11*, 173–182.

(199) Goodenough, J. B.; Hong, H.-P.; Kafalas, J. Fast Na^+-ion transport in skeleton structures. *Mater. Res. Bull.* **1976**, *11*, 203–220.

(200) Delmas, C.; Cherkaoui, F.; Nadiri, A.; Hagenmuller, P. A nasicon-type phase as intercalation electrode: $NaTi_2(PO_4)_3$. *Mater. Res. Bull.* **1987**, *22*, 631–639.

(201) Delmas, C.; Nadiri, A.; Soubeyroux, J. The nasicon-type titanium phosphates $ATi_2(PO_4)_3$ (A= Li, Na) as electrode materials. *Solid State Ion.* **1988**, *28*, 419–423.

(202) Entwistle, J.; Zhang, L.; Zhang, H.; Tapia-Ruiz, N. In *Comprehensive Inorganic Chemistry III (Third Edition)*; Reedijk, J., Poeppelmeier, K. R., Eds.; Elsevier: Oxford, 2023; pp 199–215.

(203) Chen, S.; Wu, C.; Shen, L.; Zhu, C.; Huang, Y.; Xi, K.; Maier, J.; Yu, Y. Challenges and perspectives for NASICON-type electrode materials for advanced sodium-ion batteries. *Adv. Mater.* **2017**, *29*, 1700431.

(204) Ortiz, G. F.; López, M. C.; Lavela, P.; Vidal-Abarca, C.; Tirado, J. L. Improved lithium-ion transport in NASICON-type lithium titanium phosphate by calcium and iron doping. *Solid State Ion.* **2014**, *262*, 573–577.

(205) Mariappan, C. R.; Yada, C.; Rosciano, F.; Roling, B. Correlation between micro-structural properties and ionic conductivity of $Li_{1.5}Al_{0.5}Ge_{1.5}(PO_4)_3$ ceramics. *J. Power Sources* **2011**, *196*, 6456–6464.

(206) Hou, M.; Liang, F.; Chen, K.; Dai, Y.; Xue, D. Challenges and perspectives of NASICON-type solid electrolytes for all-solid-state lithium batteries. *Nanotechnology* **2020**, *31*, 132003.

(207) Chen, M.; Hua, W.; Xiao, J.; Cortie, D.; Chen, W.; Wang, E.; Hu, Z.; Gu, Q.; Wang, X.; Indris, S., et al. NASICON-type air-stable and all-climate cathode for sodium-ion batteries with low cost and high-power density. *Nat. Commun.* **2019**, *10*, 1480.

(208) Deng, Z.; Mishra, T. P.; Mahayoni, E.; Ma, Q.; Tieu, A. J. K.; Guillon, O.; Chotard, J.-N.; Seznec, V.; Cheetham, A. K.; Masquelier, C., et al. Fundamental investigations on the sodium-ion transport properties of mixed polyanion solid-state battery electrolytes. *Nat. Commun.* **2022**, *13*, 4470.

(209) Zou, Z.; Ma, N.; Wang, A.; Ran, Y.; Song, T.; Jiao, Y.; Liu, J.; Zhou, H.; Shi, W.; He, B., et al. Relationships between Na^+ distribution, concerted migration, and diffusion properties in rhombohedral NASICON. *Adv. Energy Mater.* **2020**, *10*, 2001486.

(210) Alamo, J. Chemistry and properties of solids with the [NZP] skeleton. *Solid State Ion.* **1993**, *63*, 547–561.

(211) Karkera, G.; Reddy, M. A.; Fichtner, M. Recent developments and future perspectives of anionic batteries. *J. Power Sources* **2021**, *481*, 228877.

(212) Sandstrom, S. K.; Chen, X.; Ji, X. A review of halide charge carriers for rocking-chair and dual-ion batteries. *Carbon Energy* **2021**, *3*, 627–653.

(213) Nowroozi, M. A.; Mohammad, I.; Molaiyan, P.; Wissel, K.; Munnangi, A. R.; Clemens, O. Fluoride ion batteries – past, present, and future. *J. Mater. Chem. A* **2021**, *9*, 5980–6012.

(214) Gschwind, F.; Rodriguez-Garcia, G.; Sandbeck, D.; Groß, A.; Weil, M.; Fichtner, M.; Hörmann, N. Fluoride ion batteries: Theoretical performance, safety, toxicity, and a combinatorial screening of new electrodes. *J. Fluor. Chem.* **2016**, *182*, 76–90.

(215) Sobolev, B.; Sorokin, N. Nonstoichiometry in inorganic fluorides: 2. Ionic conductivity of nonstoichiometric $M_{1-x}R_xF_{2+x}$ and $R_{1-y}M_yF_{3-y}$ crystals (M= Ca, Sr, Ba; R are rare earth elements). *Crystallogr. Rep.* **2014**, *59*, 807–830.

(216) Anji Reddy, M.; Fichtner, M. Batteries based on fluoride shuttle. *J. Mater. Chem.* **2011**, *21*, 17059–17062.

(217) Rongeat, C.; Anji Reddy, M.; Witter, R.; Fichtner, M. Solid Electrolytes for Fluoride Ion Batteries: Ionic Conductivity in Polycrystalline Tysonite-Type Fluorides. *ACS Appl. Mater. Interfaces* **2014**, *6*, 2103–2110.

(218) Rongeat, C.; Reddy, M. A.; Witter, R.; Fichtner, M. Nanostructured Fluorite-Type Fluorides As Electrolytes for Fluoride Ion Batteries. *J. Phys. Chem. C* **2013**, *117*, 4943–4950.

(219) Dieudonné, B.; Chable, J.; Mauvy, F.; Fourcade, S.; Durand, E.; Lebraud, E.; Leblanc, M.; Legein, C.; Body, M.; Maisonneuve, V.; Demourgues, A. Exploring the $Sm_{1-x}Ca_xF_{3-x}$ Tysonite Solid Solution as a Solid-State Electrolyte: Relationships between Structural Features and F- Ionic Conductivity. *J. Phys. Chem. C* **2015**, *119*, 25170–25179.

(220) Dieudonné, B.; Chable, J.; Body, M.; Legein, C.; Durand, E.; Mauvy, F.; Fourcade, S.; Leblanc, M.; Maisonneuve, V.; Demourgues, A. The key role of the composition and structural features in fluoride ion conductivity in tysonite $Ce_{1-x}Sr_xF_{3-x}$ solid solutions. *Dalton Trans.* **2017**, *46*, 3761–3769.

(221) Sorokin, N. I. SnF_2-Based Solid Electrolytes. *Inorg. Mater.* **2004**, *40*, 989–997.

(222) Liu, L.; Yang, L.; Liu, M.; Li, X.; Shao, D.; Luo, K.; Wang, X.; Luo, Z. SnF_2-based fluoride ion electrolytes $MSnF_4$ (M = Ba, Pb) for the application of room-temperature solid-state fluoride ion batteries. *J. Alloys Compd.* **2020**, *819*, 152983.

(223) Mohammad, I.; Witter, R.; Fichtner, M.; Anji Reddy, M. Room-Temperature, Rechargeable Solid-State Fluoride-Ion Batteries. *ACS Appl. Energy Mater.* **2018**, *1*, 4766–4775.

(224) Cai, B.; Ma, Y.; Yang, B.; Liu, Y.; Xia, J.; Chen, X.; Li, Z.; Ju, M.-G. A New Descriptor for Complicated Effects of Electronic Density of States on Ion Migration. *Adv. Funct. Mater.* **2023**, *33*, 2300445.

(225) Wang, J.; Hao, J.; Duan, C.; Wang, X.; Wang, K.; Ma, C. A Fluoride-Ion-Conducting Solid Electrolyte with Both High Conductivity and Excellent Electrochemical Stability. *Small* **2022**, *18*, 2104508.

(226) Xia, T.; Li, Y.; Huang, L.; Ji, W.; Yang, M.; Zhao, X. Room-Temperature Stable Inorganic Halide Perovskite as Potential Solid Electrolyte for Chloride Ion Batteries. *ACS Appl. Mater. Interfaces* **2020**, *12*, 18634–18641.

(227) Liu, G.; Wu, Y.; Liu, Y.; Cai, B.; Dong, Y.; Zhang, S.; Zeng, H. Halide ion migration in lead-free all-inorganic cesium tin perovskites. *Appl. Phys. Lett.* **2021**, *119*, 031902.